NATIONAL ADVISORY COMMITTEE FOR AERONAUTICS

TECHNICAL NOTE 3740

PRELIMINARY WIND-TUNNEL TESTS OF TRIANGULAR AND

RECTANGULAR WINGS IN STEADY ROLL AT MACH

NUMBERS OF 1.62 AND 1.92

By Clinton E. Brown and Harry S. Heinke, Jr.

Langley Aeronautical Laboratory
Langley Field, Va.

NACA

Washington

June 1956

NATIONAL ADVISORY COMMITTEE FOR AERONAUTICS

TECHNICAL NOTE 3740

PRELIMINARY WIND-TUNNEL TESTS OF TRIANGULAR AND

RECTANGULAR WINGS IN STEADY ROLL AT MACH
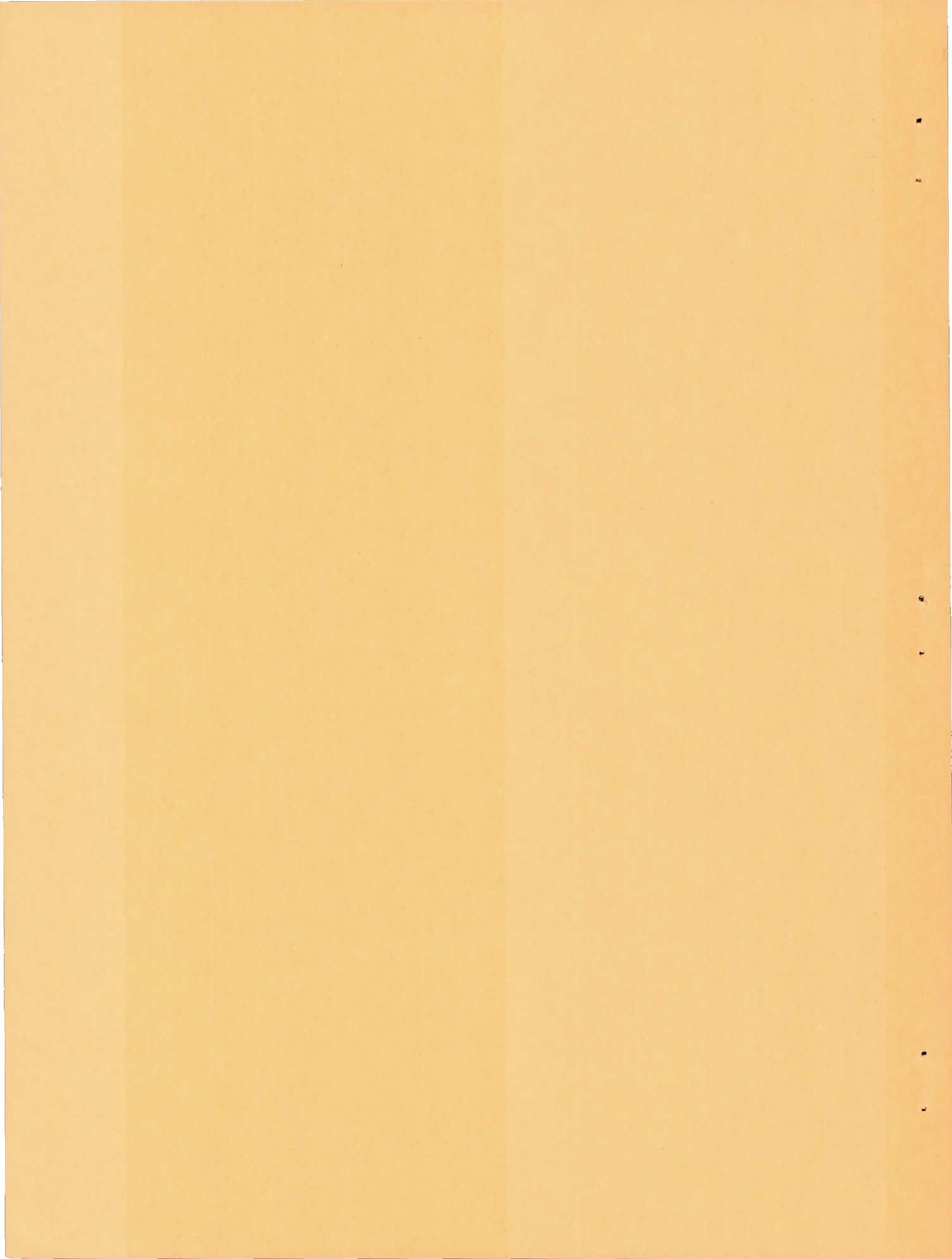
NUMBERS OF 1.62 AND 1.92[1]

By Clinton E. Brown and Harry S. Heinke, Jr.

SUMMARY

The damping-in-roll coefficients for a series of thin triangular plan-form wings and two rectangular wings have been obtained in the Langley 9-inch supersonic tunnel. The triangular-wing series consisted of nine wings of vertex angles such that a range of leading-edge positions ahead of and behind the Mach cone was obtained at two Mach numbers, 1.62 and 1.92. The rectangular wings were of aspect ratio 2.00 and 2.73. All the wings were tested in the presence of a body of revolution.

It was found that the damping in roll of the rectangular wings was very close to that predicted by linear theory for isolated wings.

The triangular wings gave results approximately 10 percent below that predicted when the wing leading edges were well ahead of or behind the Mach cone. Somewhat greater reductions in the damping coefficients from the linear theory were found when the leading edges were in the vicinity of the Mach cone.

INTRODUCTION

One of the more important factors entering in aircraft stability and control calculations is the aerodynamic resistance to roll or damping in roll. The damping in roll is generally expressed in terms of the non-dimensional parameter C_{l_p} which is the rate of change of rolling-moment coefficient with change of wing-tip helix angle $pb/2V$. The linear theory of supersonic flows has provided values of C_{l_p} for a large class of wing plan forms. (See references 1 to 5.) At the present time, rocket-powered-model tests to obtain aileron effectiveness

_____

[1]Supersedes recently declassified NACA Research Memorandum L8L30 by Clinton E. Brown and Harry S. Heinke, Jr., 1949.

are the only experimental information on rolling wings that is available for supersonic speeds. (See reference 6.)

The present tests were conducted to supply experimental C_{l_p} values for a series of wing plan forms and to check the validity of the theoretical results. The tests were made at low Reynolds numbers (R = 0.49 million to 1.30 million) at two Mach numbers, 1.62 and 1.92. Nine triangular and two rectangular wing plan forms were investigated. The triangular wings were selected so that data were obtained through the aspect-ratio range in which the leading edge passes from behind to ahead of the Mach cone emanating from the wing apexes. The aspect ratios of the two rectangular wings were 2.73 and 2.00. All wings were mounted on a slender body of revolution in which a strain-gage torque-indicating balance was installed.

The torque measurements were made at constant rotational speeds and hence the effects of oscillatory motion were not encountered. It is probable that some modification of the C_{l_p} values will be found for high-frequency rolling oscillation; theoretical analysis based on the nonstationary linearized theory will probably show that these effects become important only for frequencies approaching flutter frequencies

SYMBOLS

A	aspect ratio (b^2/S)
b	wing span, feet
$\beta = \sqrt{M^2 - 1}$	
C_l	rolling-moment coefficient (L/qSb)
C_{l_p}	damping-in-roll derivative $\left(\dfrac{\partial C_l}{\partial \dfrac{pb}{2V}}\right)$
d	maximum body diameter
ϵ	half of apex angle of wing
L	rolling moment, foot-pounds
M	free-stream Mach number
μ	Mach angle $\left(\sin^{-1} \dfrac{1}{M}\right)$
p	angular rolling velocity, radians per second

pb/2V   helix angle generated by wing tip in roll, radians

q   free-stream dynamic pressure

R   Reynolds number based on mean geometric chord of wing

S   wing area, square feet

V   free-stream velocity, feet per second

APPARATUS AND TEST MODELS

The test setup consisted of a wing-support body containing strain gages so mounted as to be sensitive to moment applied by the wings. Wires connecting the gages in a full-bridge circuit were run through the center of the model support shaft to slip rings and brushes located within the windshield and on the support bar. An electric motor rotated the model through the desired speed range by means of miter gears which permitted mounting of the motor outside of the tunnel stream. The speed of rotation was obtained from an electrical tachometer.

Figure 1 is a phantom view of the test section setup showing the relative location of the major components of the model support system. The slip rings and brushes shown are of silver-graphite composition. The strain-gage balance illustrated in figure 2 is a full-bridge circuit of four resistance wire gages attached to both sides of two beams mounted within the wing-support shell so as to read only a pure moment applied to the beams. The model was designed with the shaft or sting support cut axially into two parts with connection of the two being at the strain-gage beams only. The ends of each beam were pinned in slots machined in both shaft sections so that a moment applied through the nose section by the wings was restrained and read entirely on the strain-gage beams. The removable shell supporting the wings was attached to the nose section by the screw threads shown in figure 2.

The strain-indicator unit consisted of (1) a full-bridge circuit in parallel with the bridge composed of the strain-gage elements, (2) an oscillator to provide a 1000-cycle alternating-voltage supply for the bridge circuits, and (3) an electronic circuit in which the bridge unbalance voltages are amplified, rectified, and fed to a voltmeter which indicates the amount of unbalance. In operation the voltage unbalance is set equal to zero by adjustment of the calibrated variable resistances in the legs of the internal bridge circuit.

All but one of the triangular wings were constructed of $\frac{1}{16}$—inch—
thick brass sheet with the edges beveled symmetrically for a distance
of 3/8 inch from the edges in a normal direction. The airfoil sections
were therefore variable along the span; however, it is expected that the
airfoil section will be a second—order variable in the determination
of C_{l_p}. As a check on the possible differences due to the airfoil
section, one steel triangular wing was constructed having a diamond—
shaped airfoil section and a 45° half—apex angle. The two rectangular
wings tested were of aspect ratio 2.00 and 2.73 and used a symmetrical
6—percent—thick circular—arc airfoil section. The pertinent wing cross
sections and dimensions of the fuselage and wings are given in figure 3
and tables I and II. The fuselage shape was arbitrarily drawn to house
the strain—gage assembly. The fineness ratio of the body was 9. The
ratio of fuselage diameter to wing span varied for the different wings
tested from about 0.18 to 0.26.

The wings were held on the body by a small tongue or tab inserted in
a groove in the body. The wing—body juncture was then soldered all along
forming a very small fillet.

TEST METHODS

The rolling—moment installation was calibrated statically at intervals
during the testing to determine any possible changes in the strain—gage
constants. In these calibrations the model was subjected to rolling
moments and direct loads. The position of the loads on the model was
varied both axially and radially to obtain the effect of possible forces
due to unbalance or asymmetry. It appeared that direct loads due to
unbalance or air forces should be of no importance. As a final check on
this effect, however, the model with wings was mounted in an air dyna—
mometer and the dynamometer readings were checked against the rolling—
moment—balance readings, which also served as a check on the operation of
slip rings in the presence of vibration.

The model and support system was observed to have certain critical
speeds at which the vibration of model and support was quite severe and it
was found that unreliable data could be read at or near these speeds. It
was found that the severe vibration of the model at these critical speeds
caused a modulation of the strain—gage signal of such magnitude that the
strain—indicator amplifier circuit was operating beyond its linear range
and therefore could not average out the input signal. This same effect
developed at high rotational speeds at the end of the tests and was
attributed to gear chatter caused by wearing of the small gears in the
drive system. Checks with an oscilloscope proved, however, that the
modulation was only serious at very high rotational speeds. The data

presented herein were therefore restricted to values of the rotational speed where modulation was not present.

As it was impossible to set the wing on each side of the model with zero relative incidence, there was always a small initial tare moment at zero yaw. When this initial tare was combined with the tare moment created by the slight misalinement of the model with the tunnel stream, the total tare moment varied with the rolling angular position of the wings. This condition necessitated a determination of a zero reference moment from a faired curve of the dynamic-moment readings.

PRECISION

The precision of the data has been evaluated for each item affecting the final results in terms of the coefficient C_l and the parameter $pb/2V$.

It was found that the strain-gage-balance calibration factor was in error by ± 1.5 percent which was probably due to errors introduced in the calibration. The reading error introduced by having several operators and the inconsistency in contact resistance of the slip rings were determined to be insignificant.

Error in measurement of the span of the triangular wings was estimated to be ± 0.012 inch. This discrepancy was caused by the feathering and wearing away of the sharp tips. As the third power of the span enters into the calculation of C_l, the maximum error is about ± 0.7 percent. Error in $pb/2V$ from this source is negligible. In all cases the wing area includes the area buried in the body.

Error in measurement of the apex angle gave an uncertainty in wing area such that an error of about 0.4 percent is present in values of C_l.

Measurements of the rolling velocity were in error by ± 10 rpm in the test range of 2500 rpm and contributed a maximum error in $pb/2V$ of ± 0.4 percent.

The above estimates were made on the basis of static conditions. The errors arising from vibration of the model and from forces applied by the supersonic stream are difficult to evaluate. It is known, however, that at or near critical rotational speeds serious scattering occurred and therefore vibration did affect the readings. As a result of this unknown factor, the data are probably not as accurate as the static estimates would indicate. It is felt on the basis of the observed scatter in the data, that the errors should be less than ± 3.0 percent.

The results are presented for the average free-stream Mach numbers of 1.62 and 1.92 both having a surveyed variation of about ± 0.01.

The average Reynolds number was computed for the mean geometric chord of each wing and is specified on each test plot. Due to slight variation in tunnel temperature and pressure during the test runs, the average values varied by about ±4000.

RESULTS AND DISCUSSION

Within the accuracy of the test data, the values of the rolling-moment coefficient for all wings were found to be proportional to the rolling velocity. The parameter C_{l_p} is therefore independent of rolling velocity as predicted by linear theory. The collected values of C_{l_p} for the triangular series are plotted in figure 4 in a manner suggested by the linear theory for wings in steady roll; the abscissa is the parameter $\tan \epsilon / \tan \mu$ which describes the position of the leading edges relative to the Mach cone from the wing apex. Values of $\tan \epsilon / \tan \mu$ less than one produce the so-called subsonic leading-edge condition and values higher than one, the supersonic leading-edge condition. The difference lies in the types of pressure distributions predicted theoretically for the two cases. Plotted as the ordinate is the quantity $\sqrt{M^2 - 1}\, C_{l_p}$. The figure plotted in this manner allows the theoretical values for isolated wings to be represented by a single curve independent of Mach number. (See reference 1.)

The experimental points for each Mach number produce a rather broken curve in the range of $\tan \epsilon / \tan \mu$ near one. It appears unusual that the breaks occur for the wings having values of ϵ of approximately 30° and 35°. When this effect was first noted, the wing areas and calculations for the wings were rechecked and one check run was made for the $\epsilon = 30^{\circ}$ wing at $M = 1.92$; however, no plausible explanation of the breaks could be found. As the uncertainty of the data is estimated to be less than that indicated by the breaks in the curve, it is felt that the deviations from a smooth variation actually exist and perhaps are caused by interference between the wing and body; it might be noted that the deviations occur for values of $\tan \epsilon / \tan \mu$ near 1.0 where the flow over the leading edges is of transonic character. The variations which occur in the ratio of fuselage diameter to wing span were investigated as a possible cause of the deviations; however, it was not considered possible that the small variation in the wing proportions could produce the changes experienced. In any event, a smooth curve can be drawn through the data for which the maximum deviation of the points from a mean curve at both Mach numbers will be of the order of ±5 percent.

The effect of body interference on the damping forces is not known, however, it might be expected that the body would produce a certain amount of increased pressure over the wing root sections to compensate somewhat for the wing area buried in the fuselage. If this were so, the data should be expected to conform more closely with theory. It is probable that the observed discrepancy between the theory and experiment (roughly 10 percent) is caused by boundary-layer thickening or separation. Tests at higher Reynolds numbers should clarify the situation.

The values of C_{l_p} for the two triangular wings of $45°$ semivertex angle but different airfoil section were found to be identical within the experimental accuracy. It thus appears that the effect of section, at least for the very thin wings tested, is negligible.

In figure 5 the results for the two rectangular wings are plotted with the curve predicted by linear theory for isolated wings. (See reference 2.) The agreement is surprisingly good considering the presence of a fuselage in the experimental results. Although the buried wing area for the low-aspect-ratio wing is approximately 30 percent, this area is in a region of low effectiveness and considering the theoretical pressure distribution should only reduce the rolling moment by about 5 percent. It is possible that the presence of the body can give rise to increased damping pressures over wing root sections.

The data obtained for all the wings tested are presented in figures 6 to 9. The figures indicate the range of $pb/2V$ values attained and show the amount of scatter. Values of the ratio of fuselage diameter to wing span are given on each chart.

CONCLUSIONS

Wind-tunnel tests at Mach numbers $M = 1.62$ and 1.92 of the damping-in-roll characteristics of a series of triangular plan-form wings and two rectangular wings enabled the following conclusions to be reached:

(1) The triangular wings gave results approximately 10 percent below that predicted when the wing leading edges were well ahead of or behind the Mach cone. Somewhat greater reductions in the damping coefficients from the linear theory were found when the leading edges were in the vicinity of the Mach cone.

(2) The damping in roll of rectangular wings appears to be predicted quite accurately by the linear theory at least in the range of aspect ratios tested ($A \sqrt{M^2 - 1}$ from 2.5 to 4.5).

Langley Aeronautical Laboratory,
    National Advisory Committee for Aeronautics,
        Langley Field, Va., Jan. 11, 1949.

REFERENCES

1. Brown, Clinton E., and Adams, Mac C.: Damping in Pitch and Roll of Triangular Wings at Supersonic Speeds. NACA Rep. 892, 1948. (Supersedes NACA TN 1566.)

2. Lagerstrom, P. A., and Graham, Martha E.: Some Aerodynamic Formulas in Linearized Supersonic Theory for Damping in Roll and Effect of Twist for Trapezoidal Wings. Rep. No. SM-13200, Douglas Aircraft Co., Inc., March 12, 1948.

3. Ribner, Herbert S.: The Stability Derivatives of Low-Aspect-Ratio Triangular Wings at Subsonic and Supersonic Speeds. NACA TN 1423, 1947.

4. Ribner, Herbert S., and Malvestuto, Frank S., Jr.: Stability Derivatives of Triangular Wings at Supersonic Speeds. NACA Rep. 908, 1948. (Supersedes NACA TN 1572.)

5. Jones, Arthur L., and Alksne, Alberta: The Damping Due to Roll of Triangular, Trapezoidal, and Related Plan Forms in Supersonic Flow. NACA TN 1548, 1948.

6. Sandahl, Carl A.: Free-Flight Investigation of the Rolling Effectiveness of Several Delta Wing-Aileron Configurations at Transonic and Supersonic Speeds. NACA RM L8D16, 1948.

TABLE I.— TRIANGULAR-WING DIMENSIONS

ϵ (deg)	Total wing area (sq ft)	Span (ft)
20.2	0.074	0.330
25.0	.080	.386
28.2	.074	.397
30.5	.063	.387
33.1	.061	.398
35.4	.059	.410
37.6	.052	.398
40.3	.050	.410
44.6	.036	.378
45.1	.036	.382

TABLE II.— RECTANGULAR-WING DIMENSIONS

Aspect ratio	Total wing area (sq ft)	Span (ft)	Chord (ft)
2.00	0.040	0.283	0.142
2.73	.055	.389	.142

1 Strain-gage model
2 Windshield
3 Bearing housing
4 Slip rings
5 Gear box
6 Drive motor
7 Support beam

L-57005
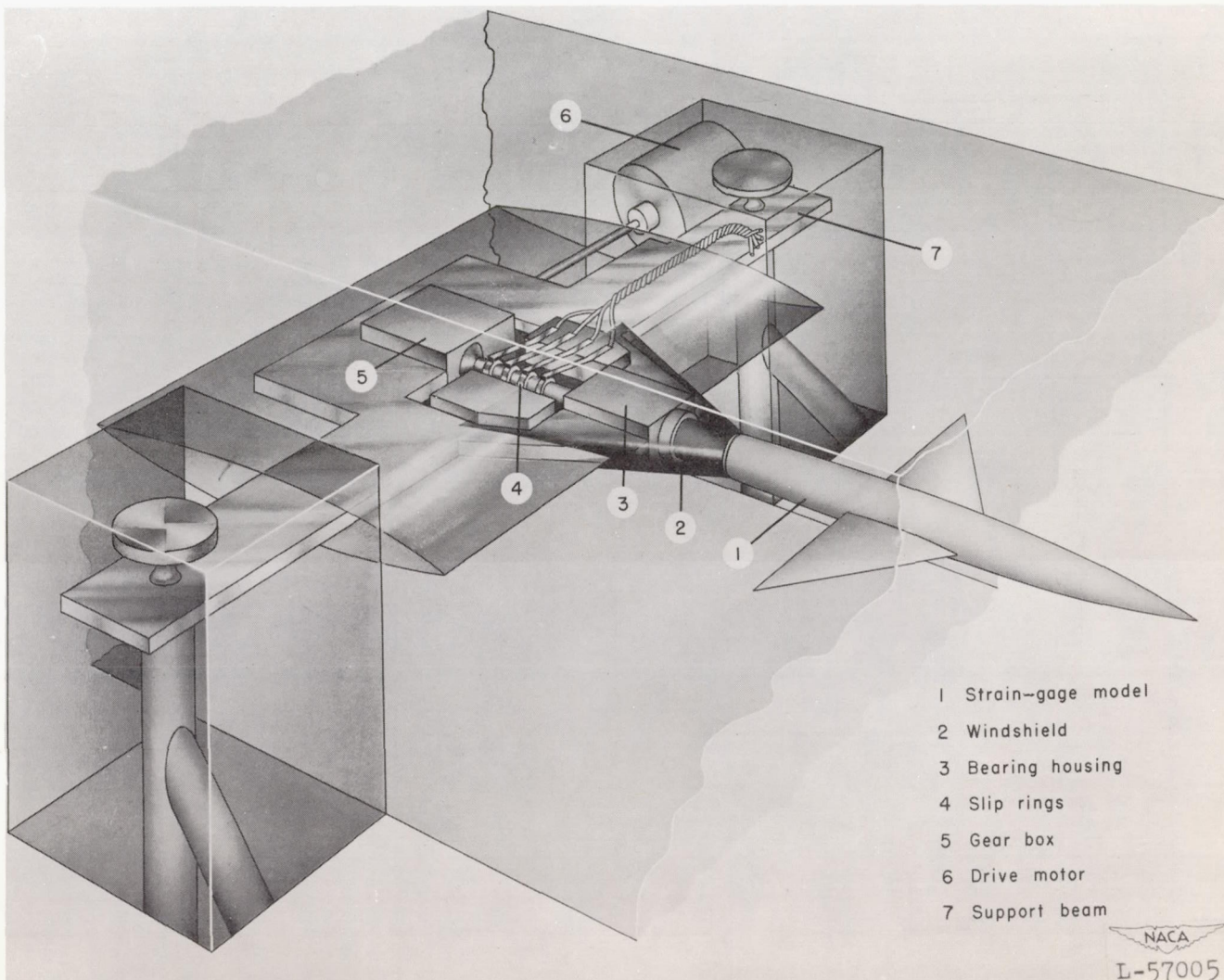
Figure 1.— Damping-in-roll test setup.

1 Strain-gage beams
2 Strain gages
3 Wing
4 Removable shell
5 Model sting support
6 Electrical connectors
7 Windshield
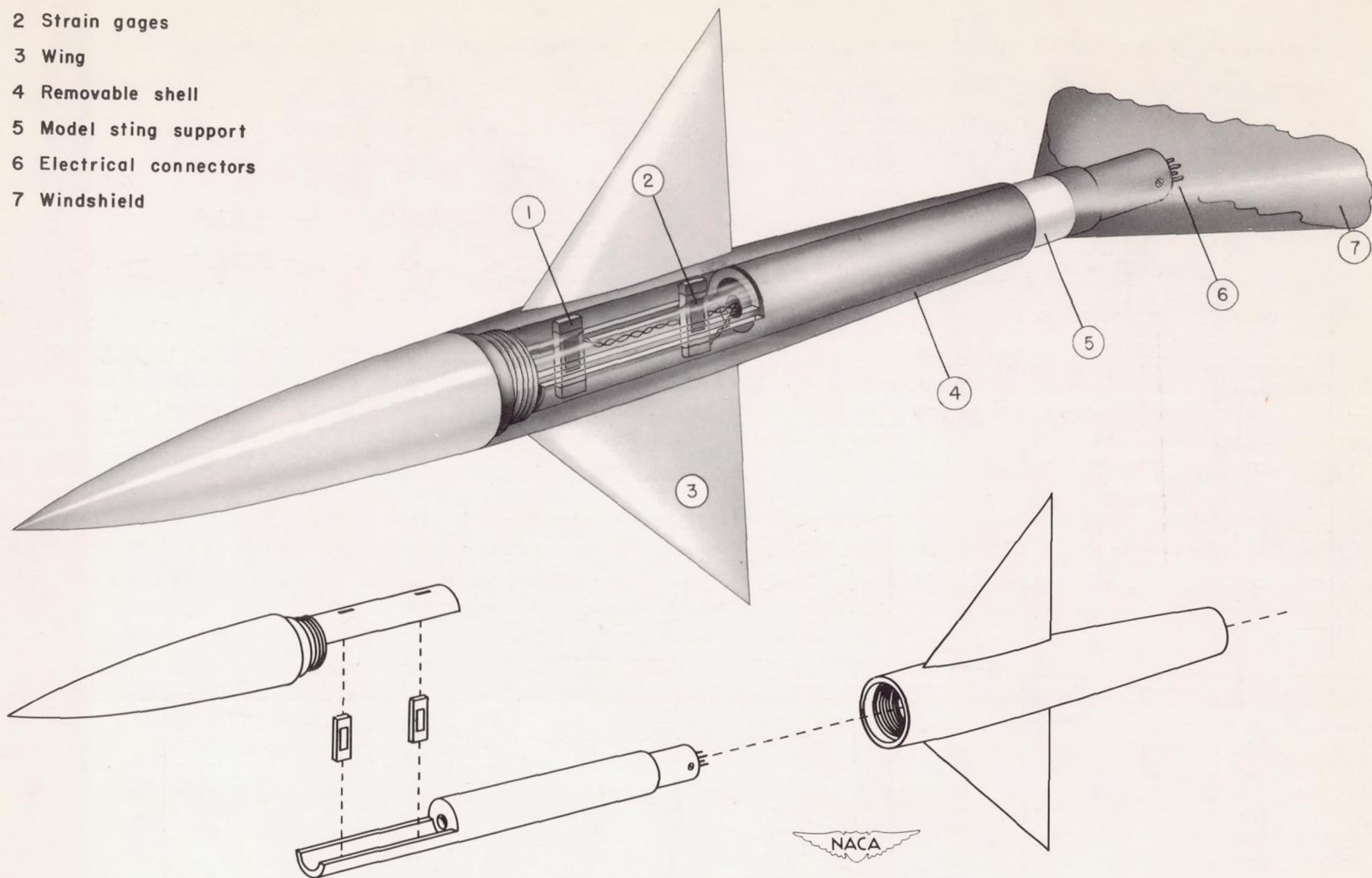
Figure 2.— Strain-gage model showing internal balance.

Station 0 Station 3.250 Station 3.438 Station 8.475

Fuselage Ordinates	
Station	Radius
0.000	0.000
.200	.050
.400	.096
.600	.137
1.000	.208
1.400	.267
1.800	.315
2.200	.355
2.600	.390
3.000	.420
3.250	.434
3.600	.446
4.000	.449
4.400	.450
4.800	.450
5.200	.449
5.475	.446
5.800	.441
6.200	.435
6.600	.428
7.000	.420
7.400	.410
7.800	.398
8.475	.325

ε

B B A A

Rectangular wings. Six percent circular arc.

Triangular wings. $\varepsilon = 20.2°$ to $\varepsilon = 44.6°$

Triangular wing. $\varepsilon = 45°$

4.9°   2.3°   0.04C

1.700   0.375   .064   0.375   0.5C

B-B   A-A   Streamwise Cross section.

NACA

Figure 3.— Fuselage ordinates and wing cross sections. All dimensions are in inches.
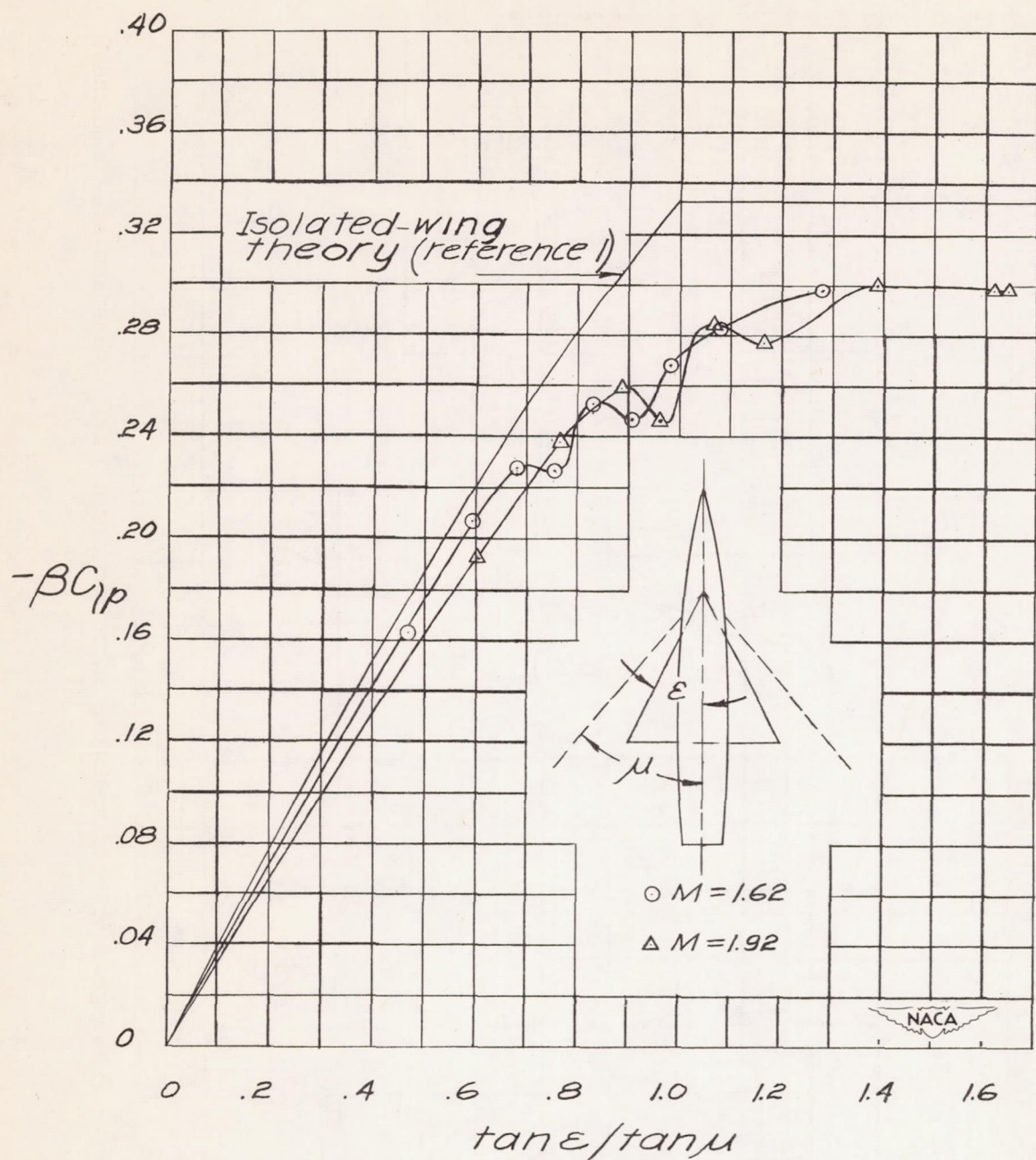
Figure 4.— Damping in roll of triangular wings on a body of revolution.
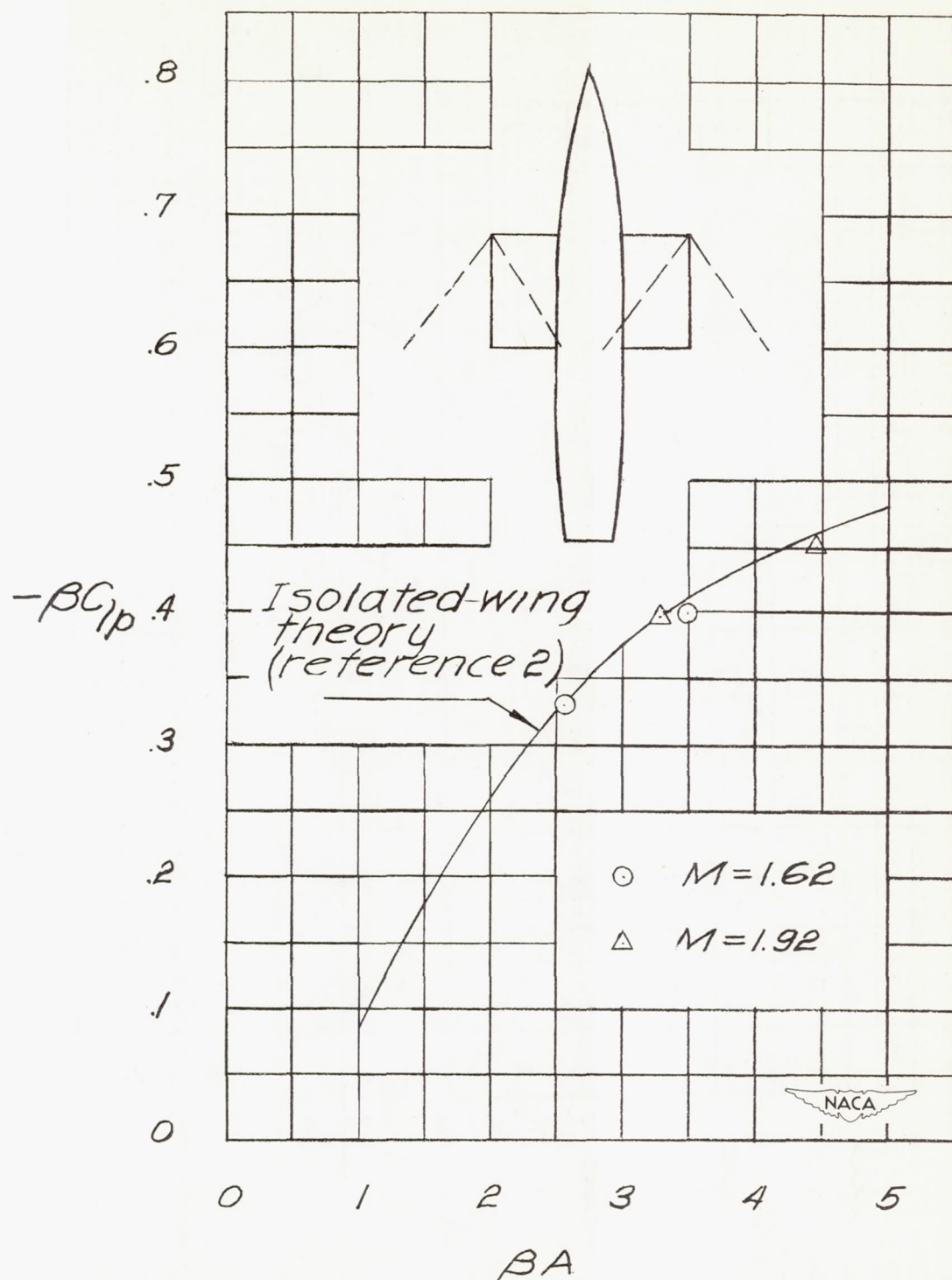
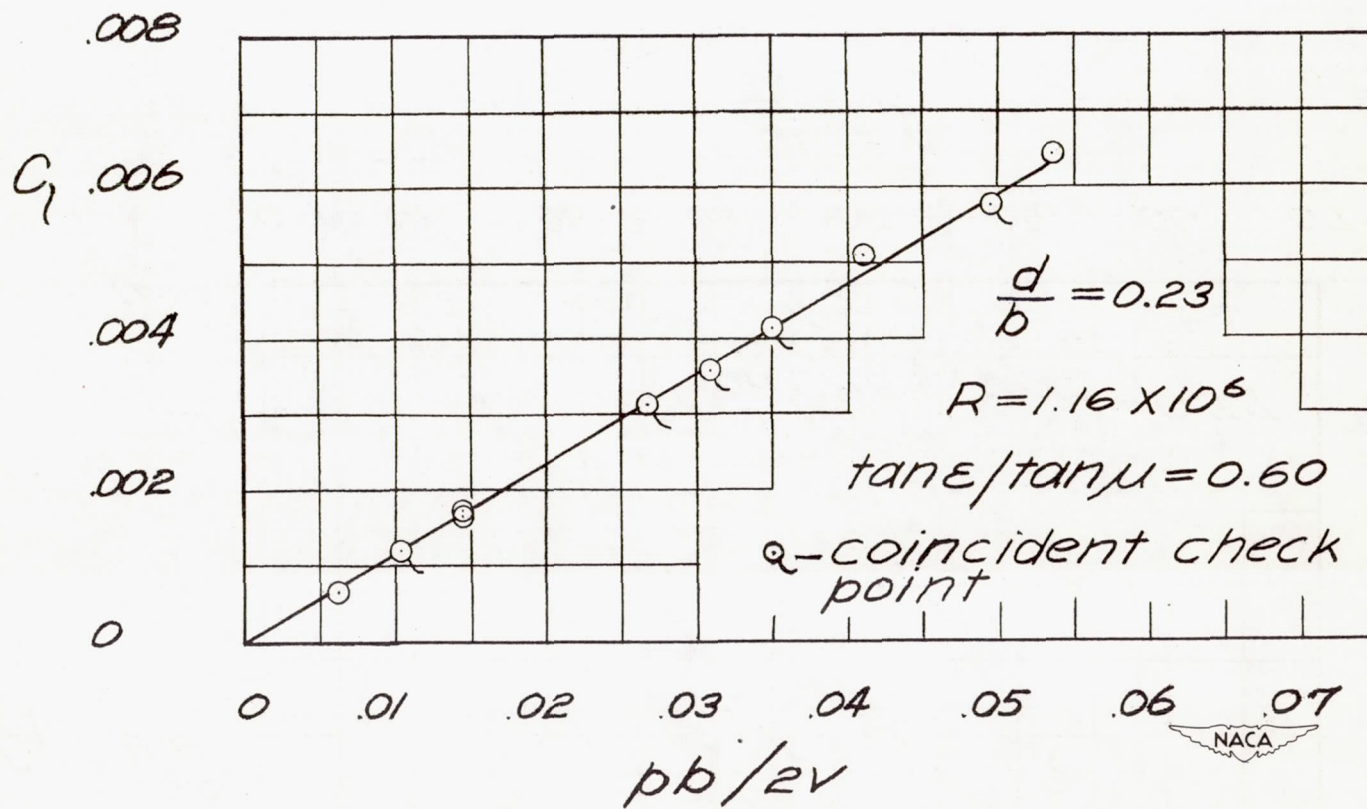Figure 5.– Damping in roll of rectangular wings on a body of revolution.
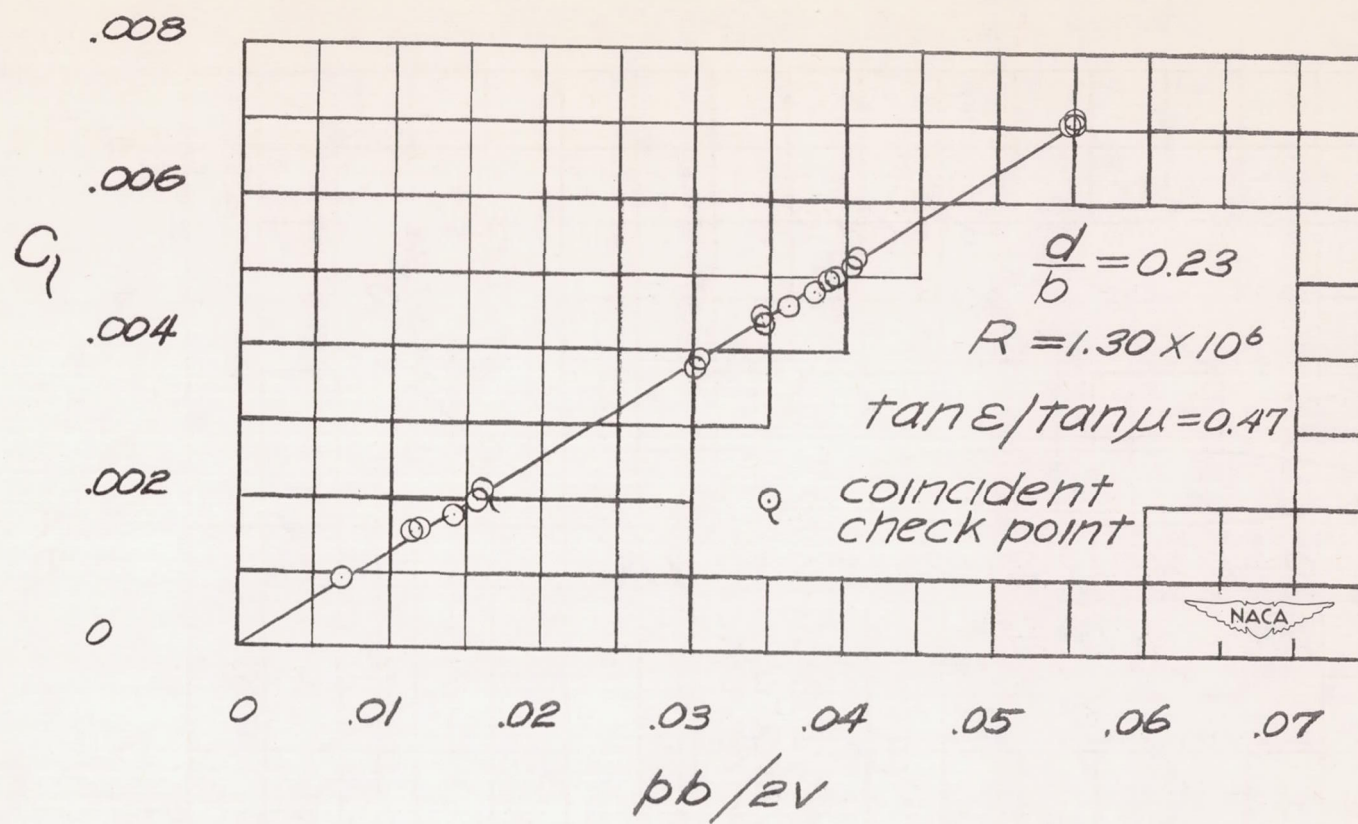
(a) Wing $\epsilon = 20.2°$.

Figure 6.— Triangular-wing variation of rolling-moment coefficient with wing–tip helix angle.
M = 1.62.
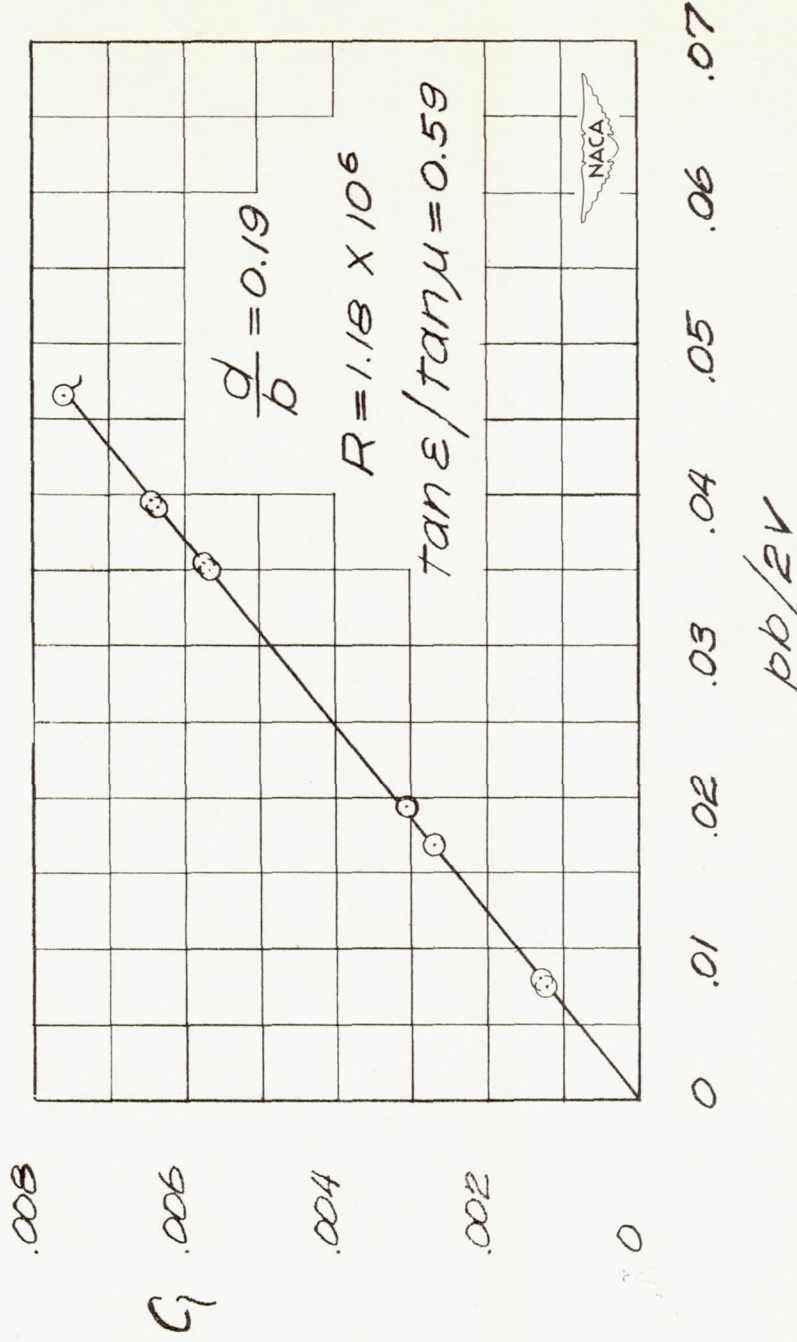
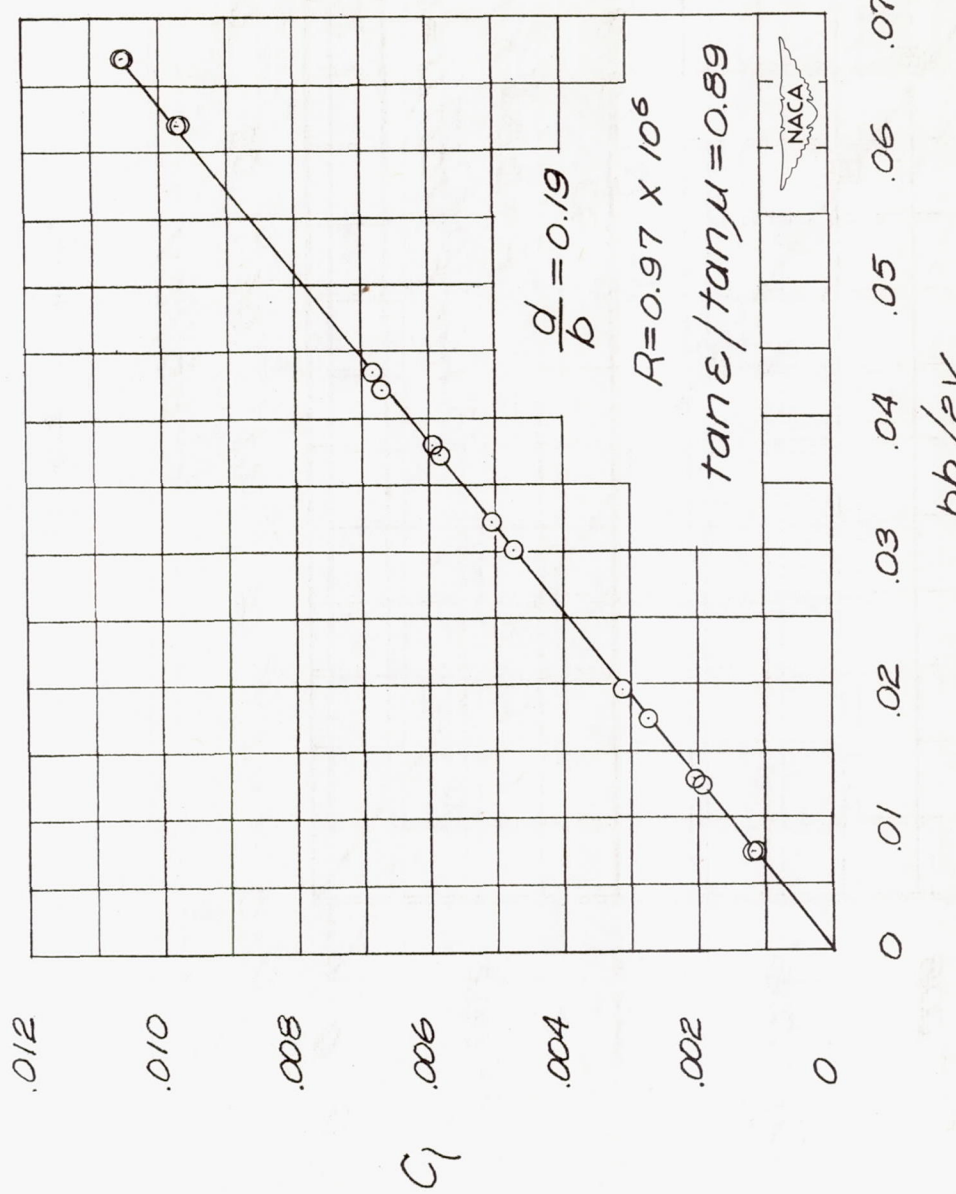(b) Wing $\epsilon = 25.0^\circ$.

Figure 6.— Continued.
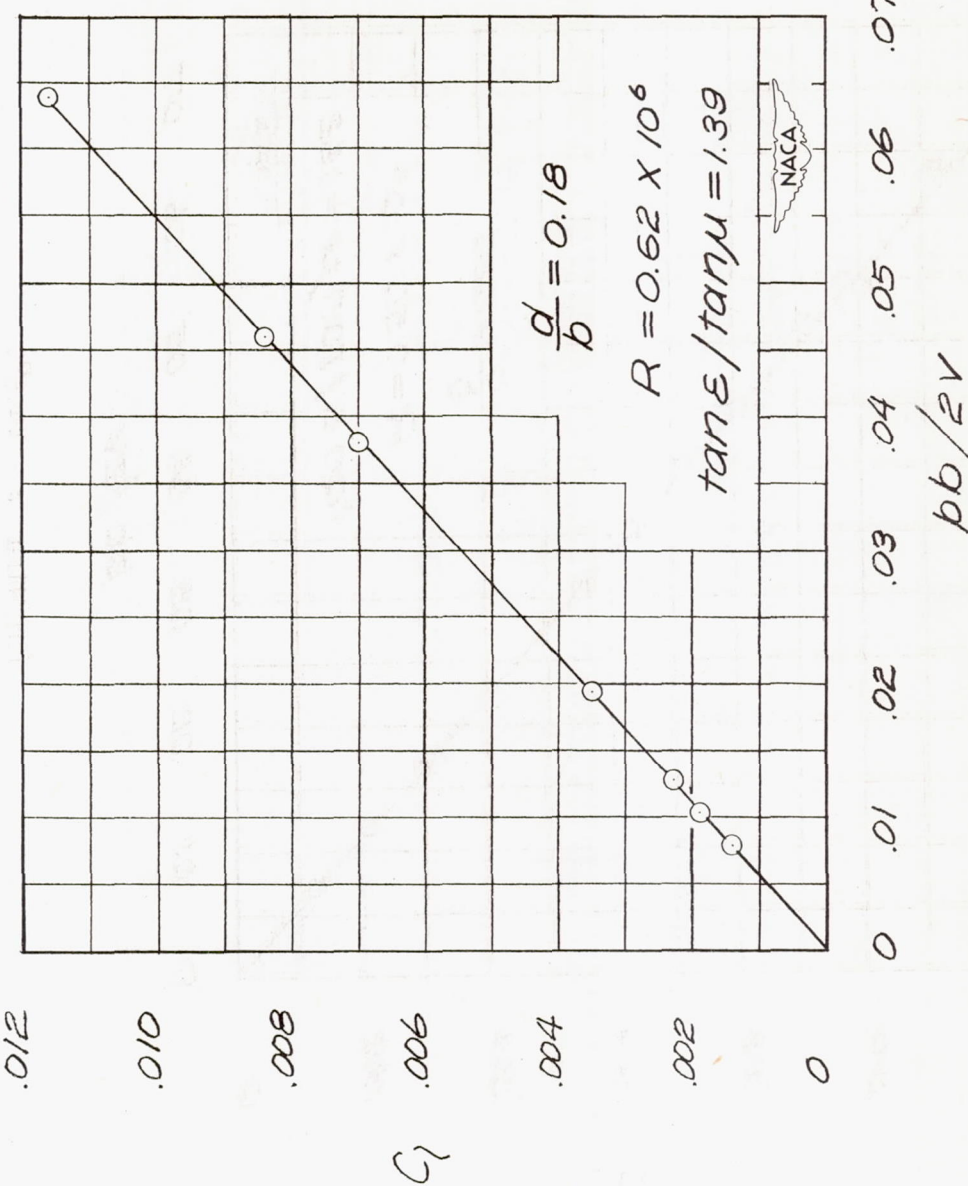
3L
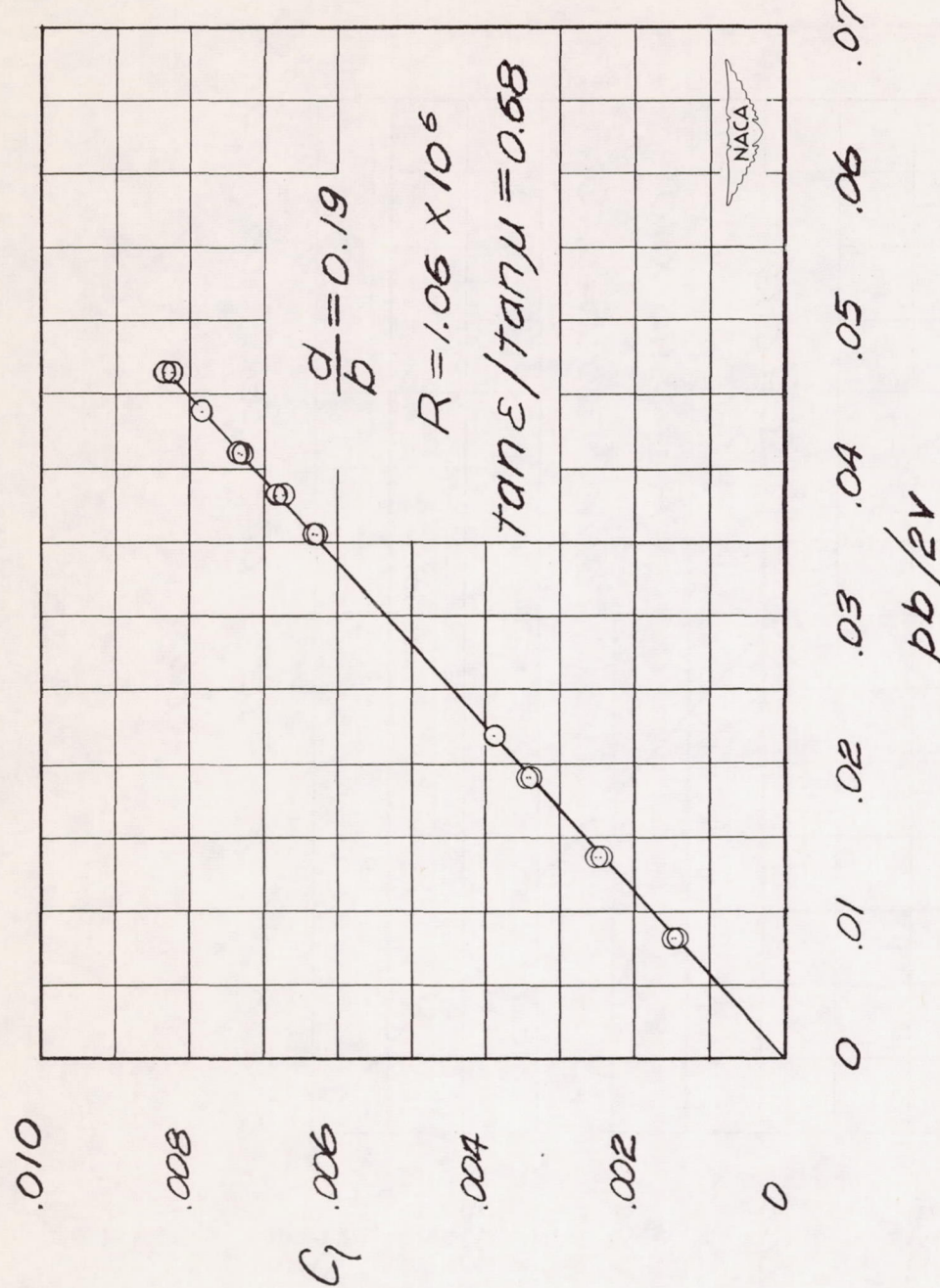
(c) Wing $\epsilon = 28.2°$.

Figure 6.— Continued.

(d) Wing ε = 30.5°.

Figure 6.— Continued.

$$\frac{d}{b}=0.19$$

$$R=0.87\times10^{6}$$

$$\tan\epsilon/\tan\mu=0.83$$

(e) Wing $\epsilon = 33.1°$.

Figure 6.– Continued.

$\frac{d}{b}=0.18$

$R=0.82\times10^{6}$

$\tan\epsilon/\tan\mu=0.91$
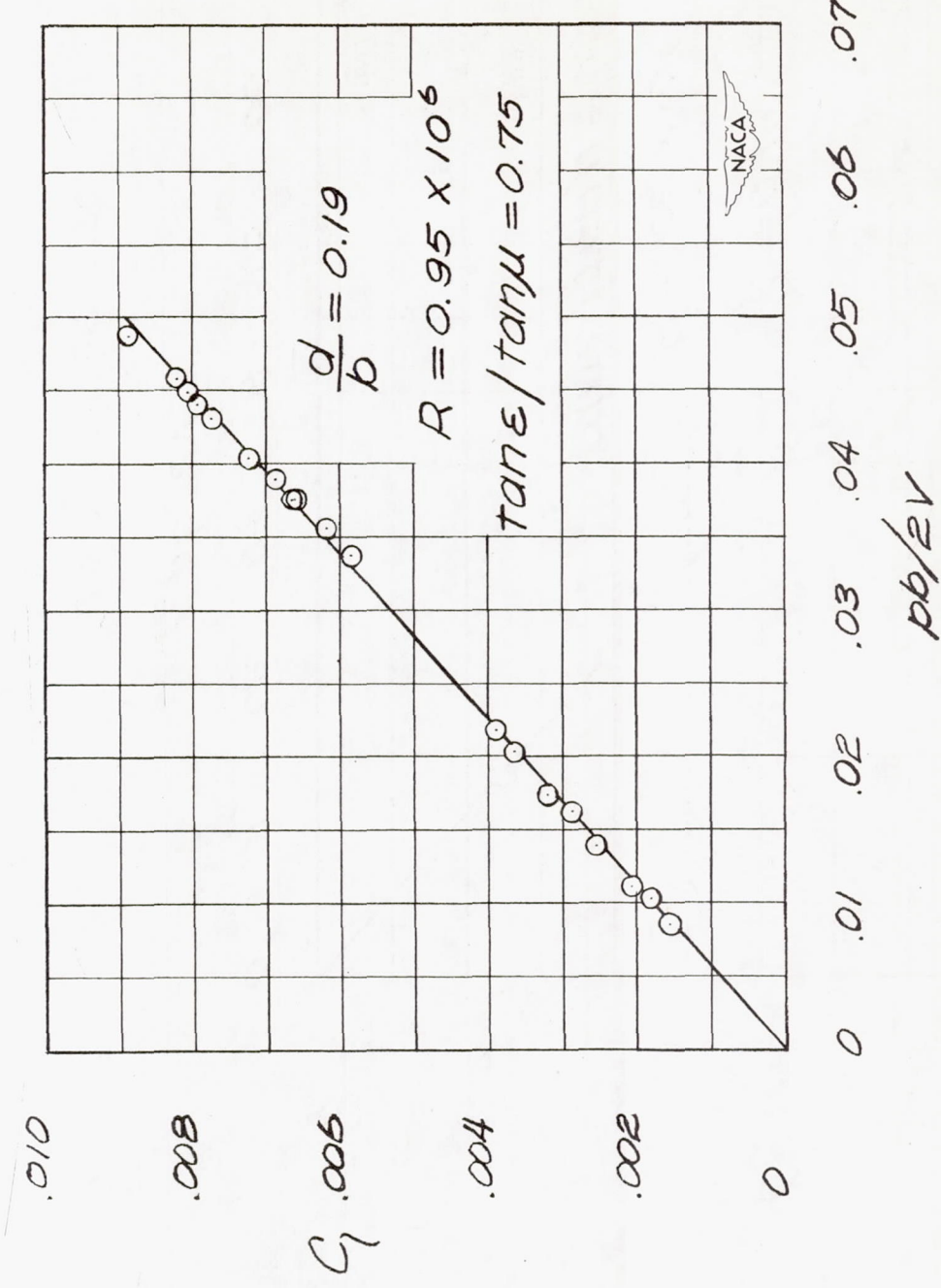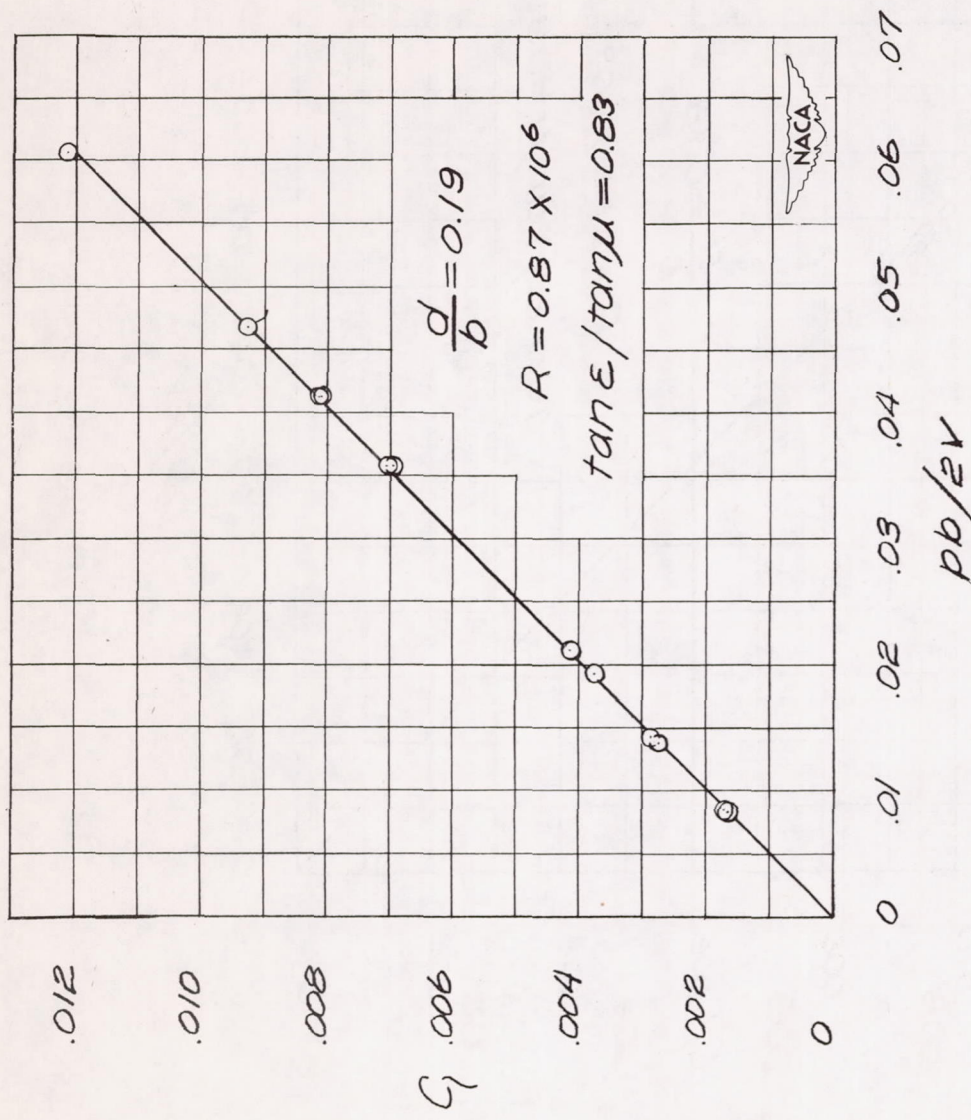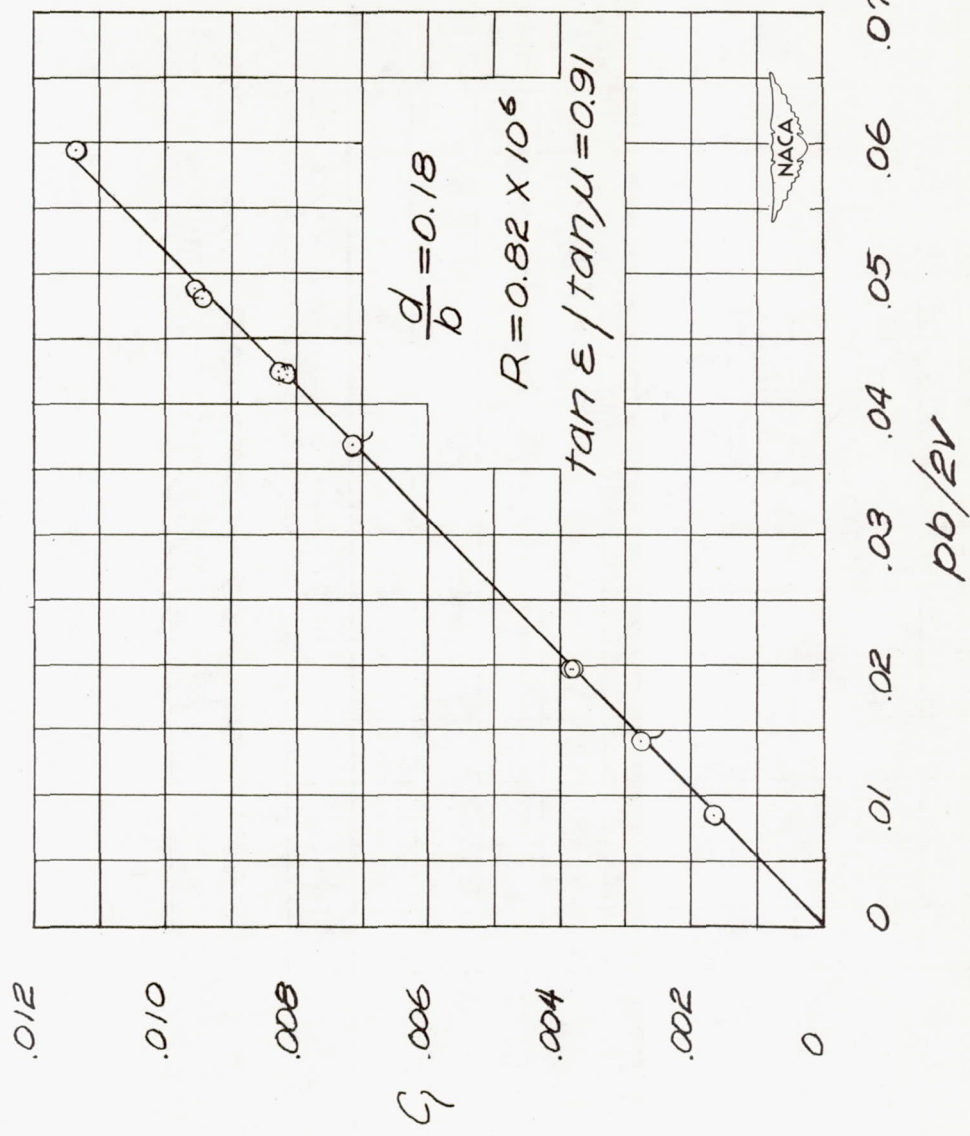
(f) Wing $\epsilon = 35.4°$.

Figure 6.— Continued.

$\dfrac{d}{b} = 0.19$

$R = 0.74 \times 10^6$

$\tan \epsilon / \tan \mu = 0.98$
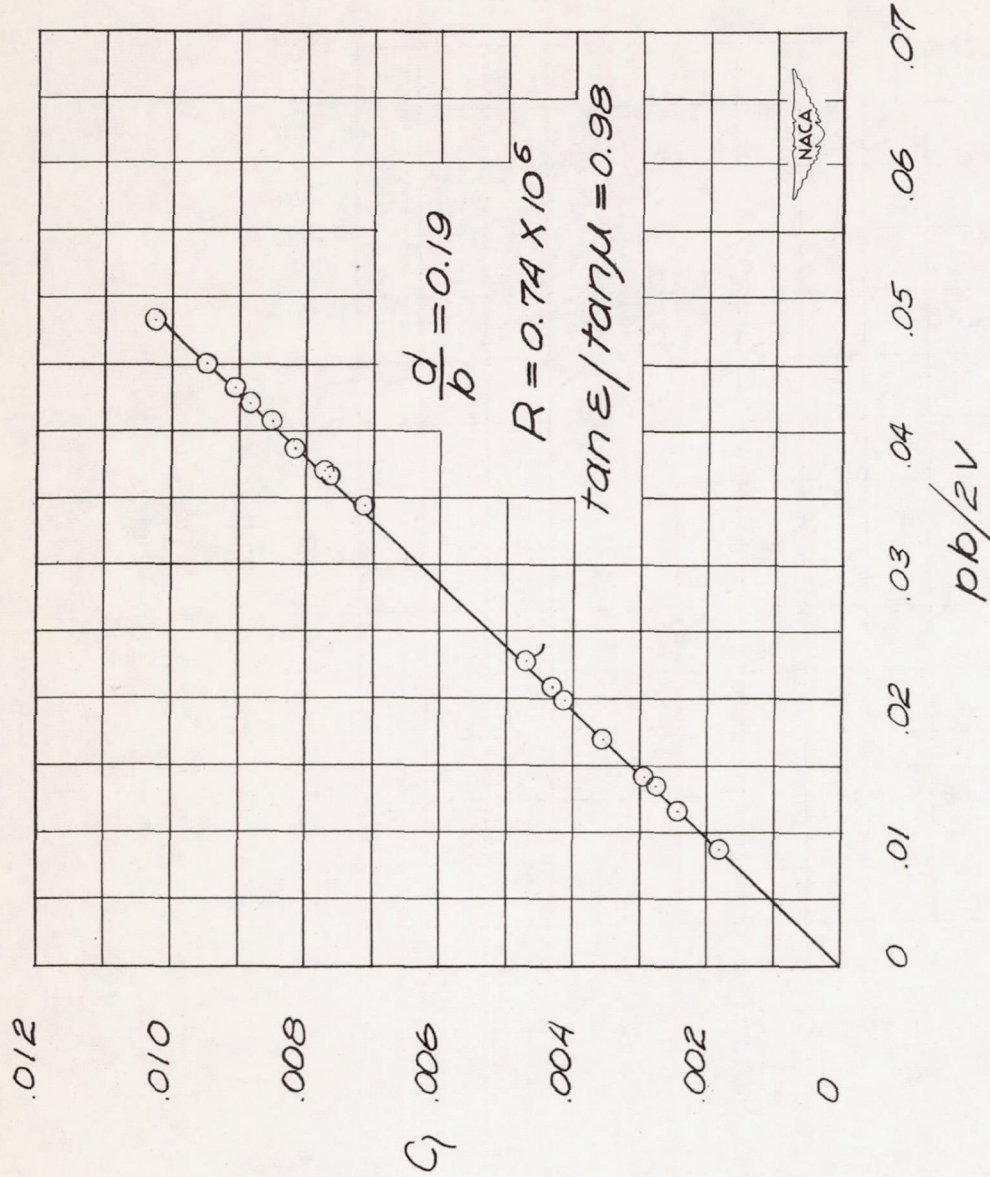
(g) Wing $\epsilon = 37.6°$.

Figure 6.— Continued.
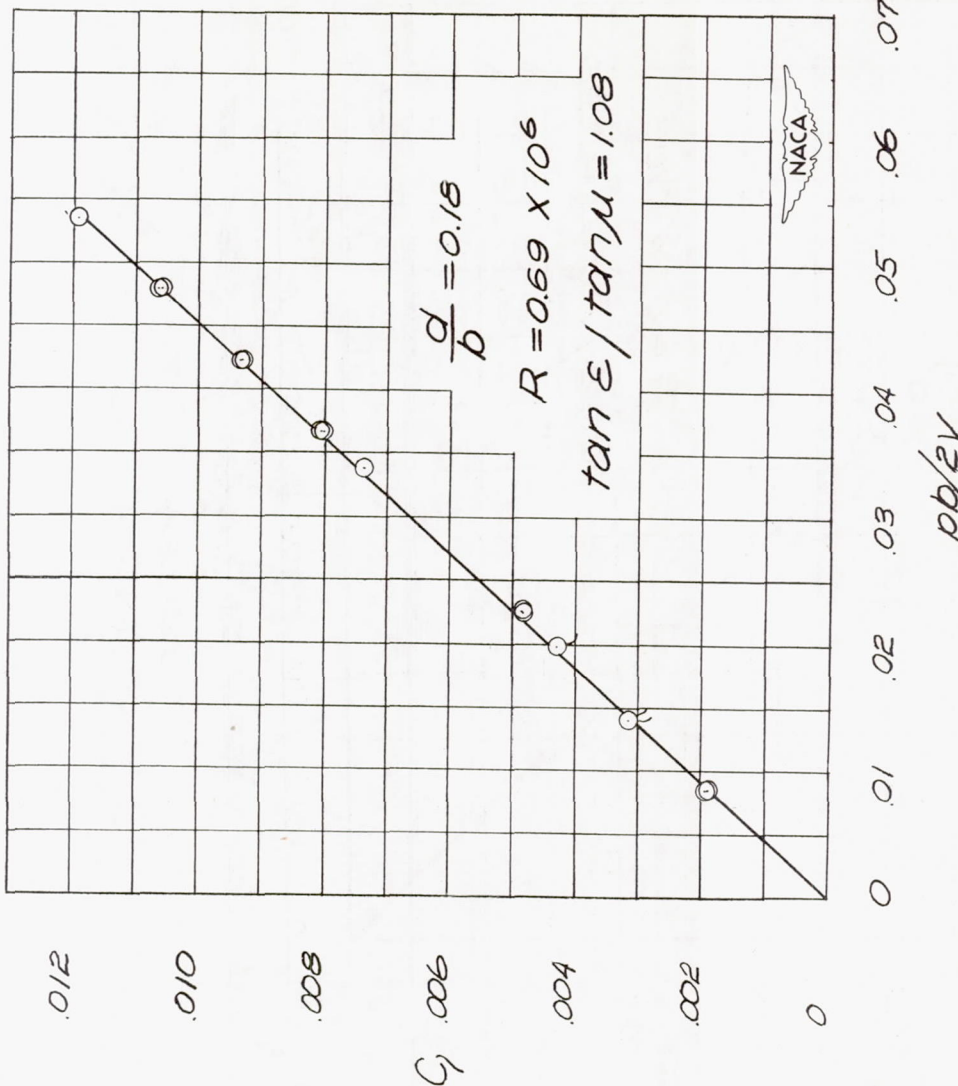
(h) Wing ε = 40.3°.

Figure 6.— Continued.
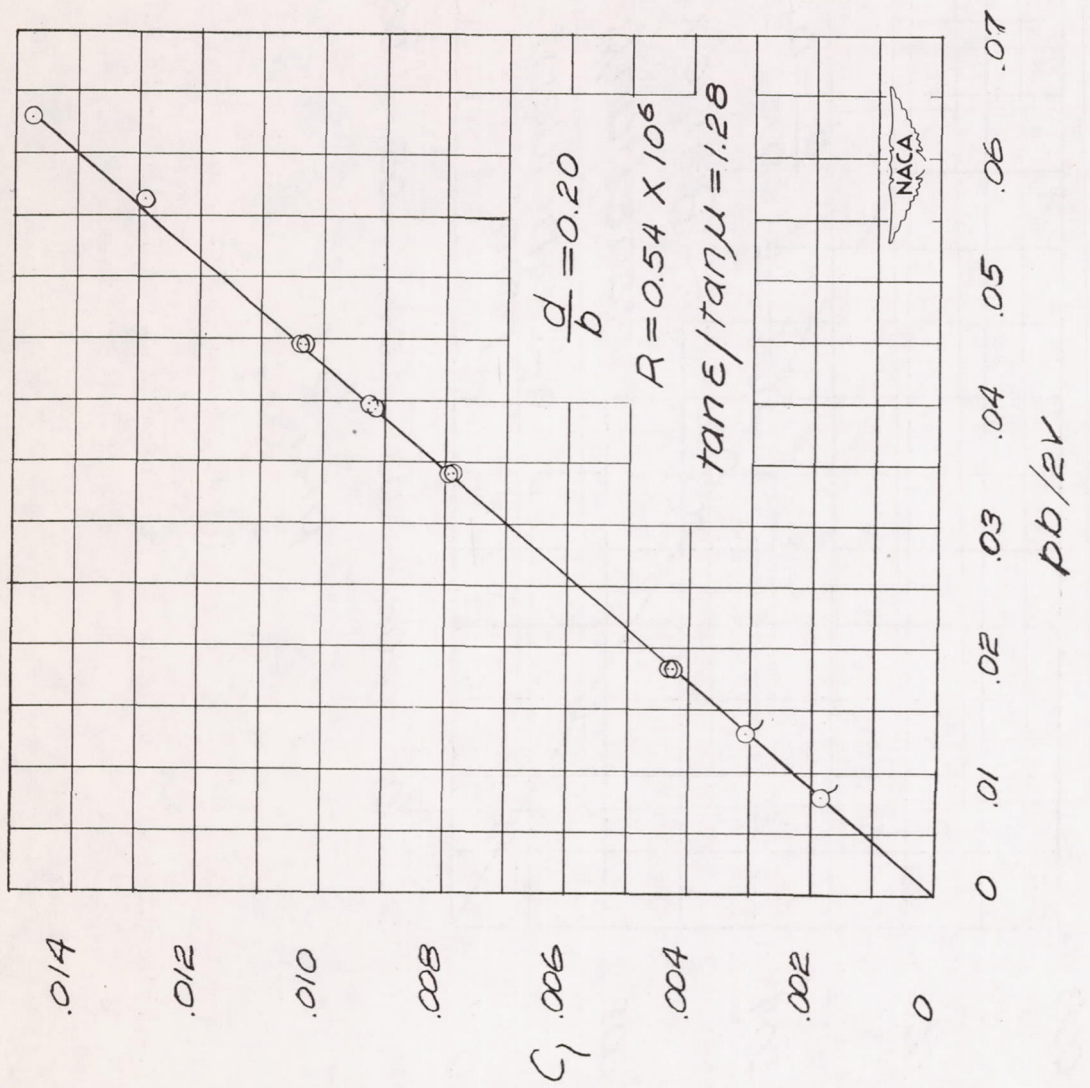
(i) Wing $\epsilon = 45.1°$.

Figure 6.— Concluded.

(a) Wing $\epsilon = 20.2°$.

Figure 7.— Triangular-wing variation of rolling-moment coefficient with wing-tip helix angle. M = 1.92.
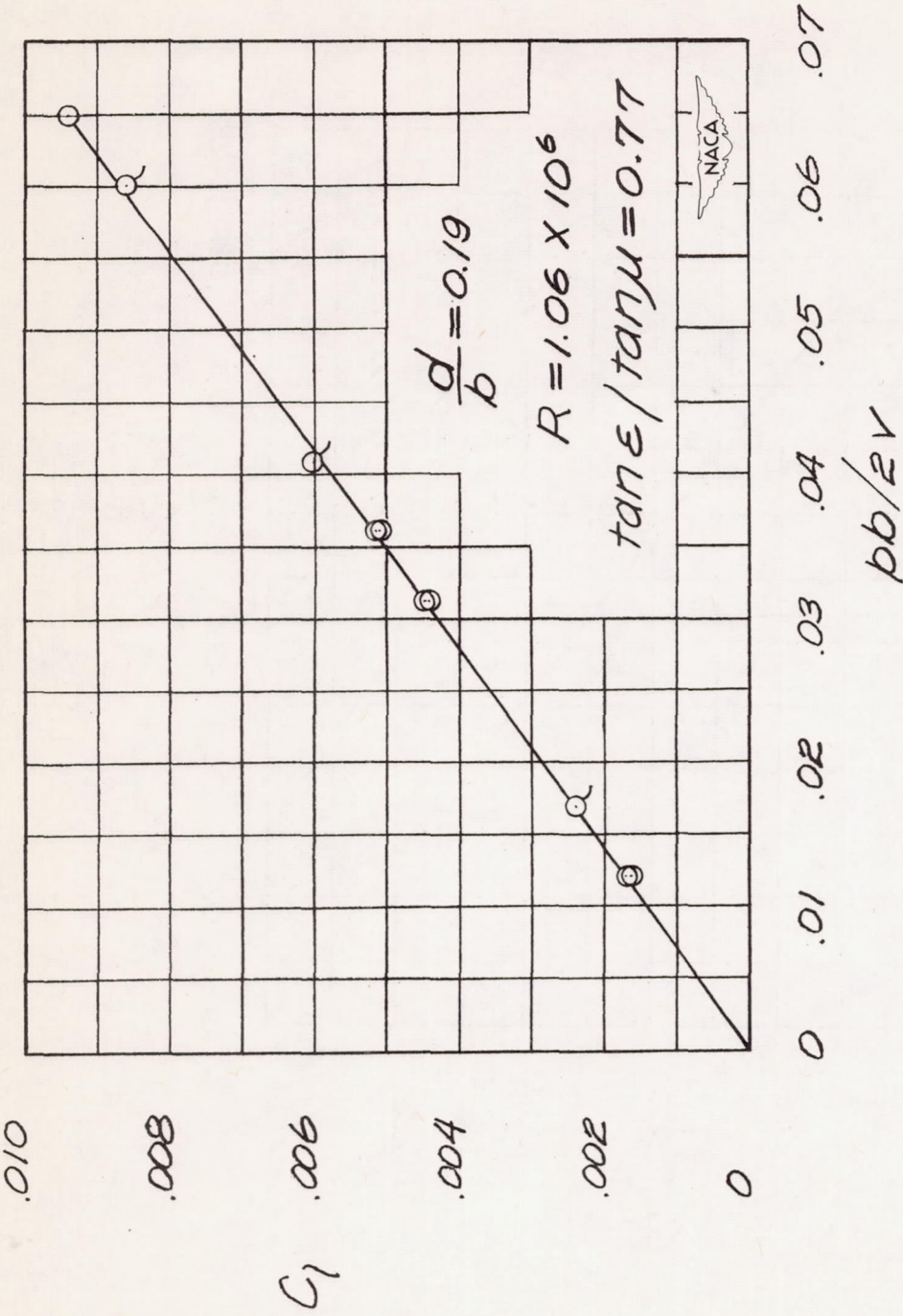
(b) Wing $\epsilon = 25.0°$.

Figure 7.— Continued.

(c) Wing ε = 28.2°.

Figure 7.— Continued.
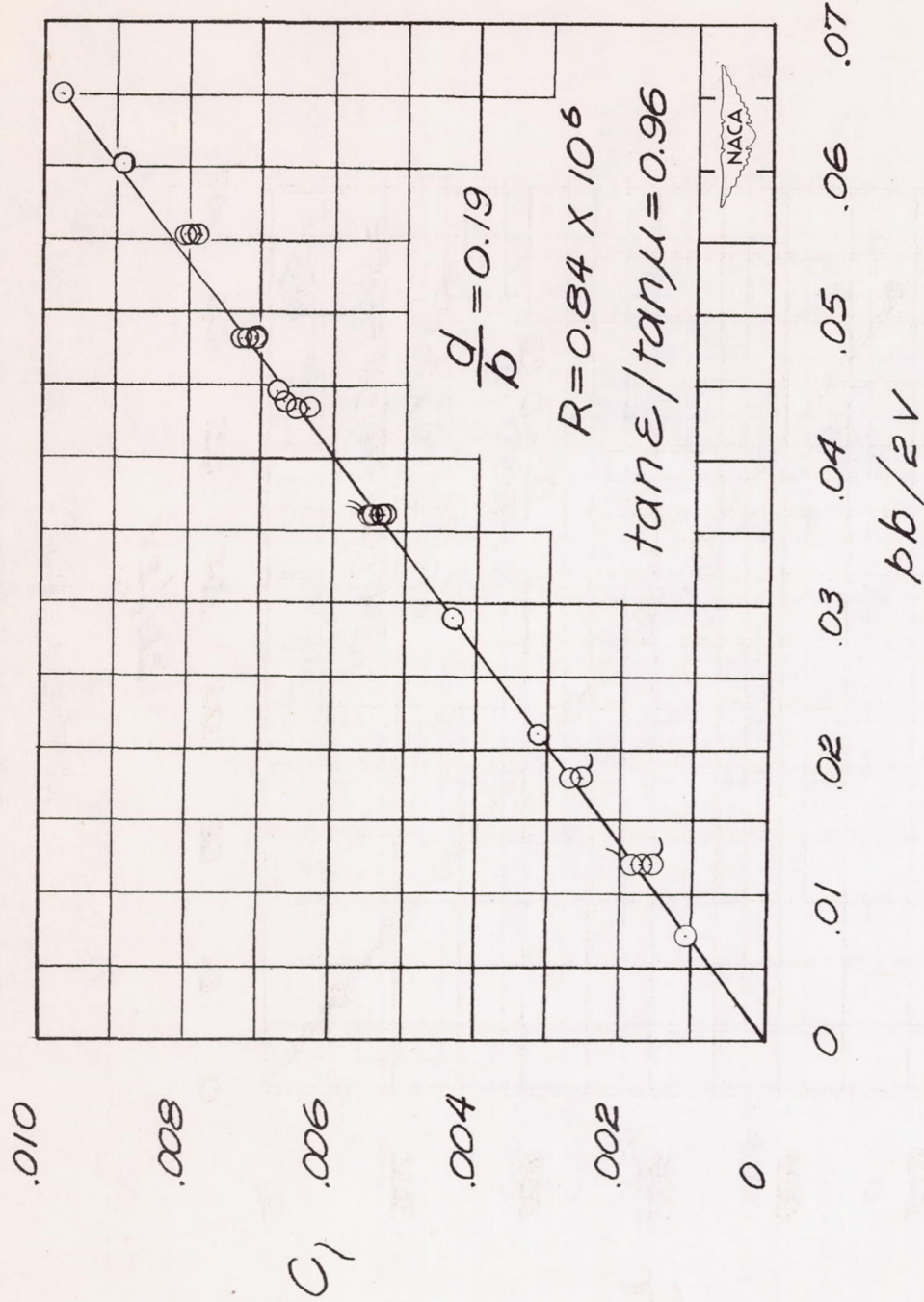
(d) Wing ε = 30.5°.

Figure 7.— Continued.

$$\frac{d}{b} = 0.19$$

$$R = 0.79 \times 10^6$$

$$\tan \varepsilon / \tan \mu = 1.07$$
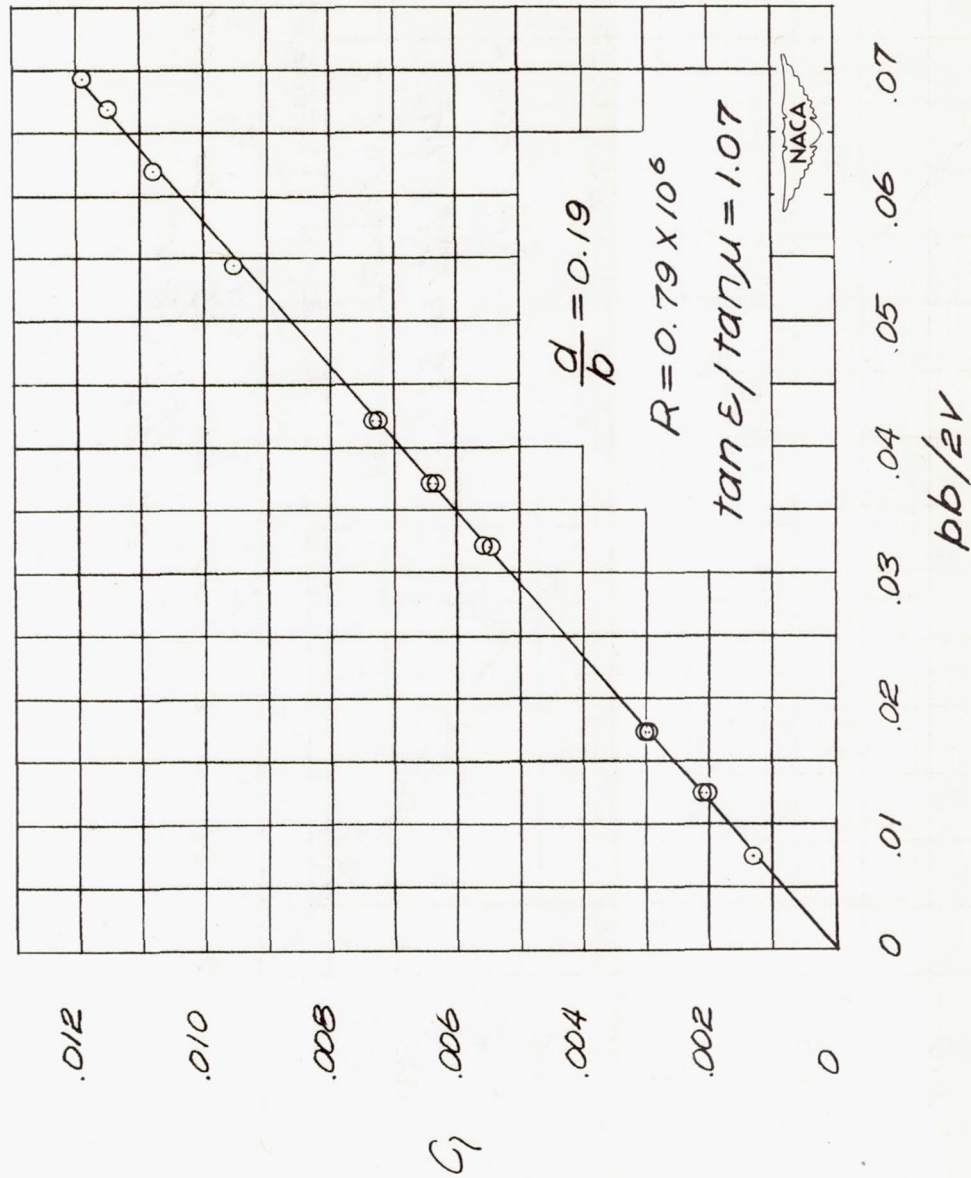
(e) Wing $\varepsilon = 33.1°$.

Figure 7.— Continued.
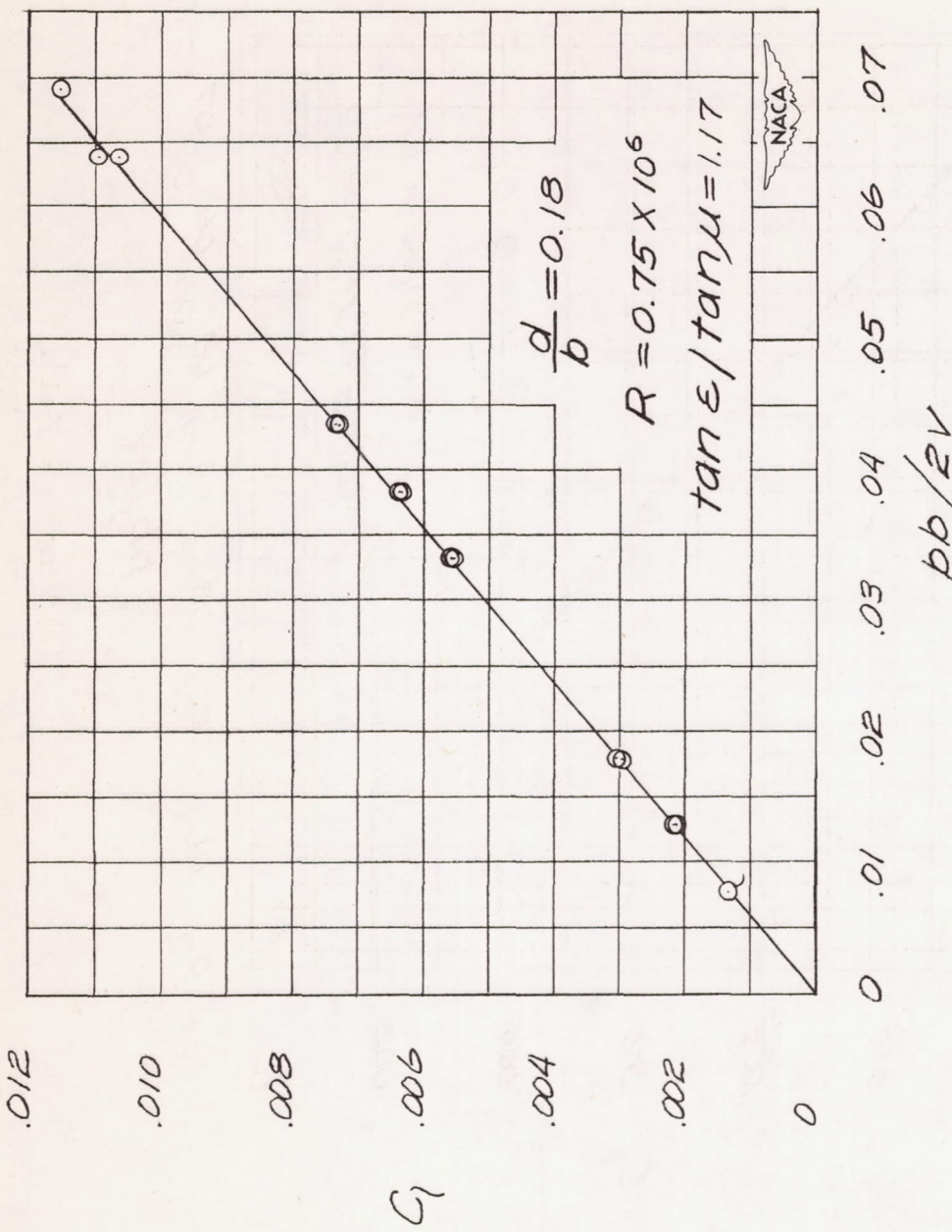
(f) Wing ε = 35.4°.

Figure 7.— Continued.

(g) Wing ε = 40.3°.

Figure 7.– Continued.
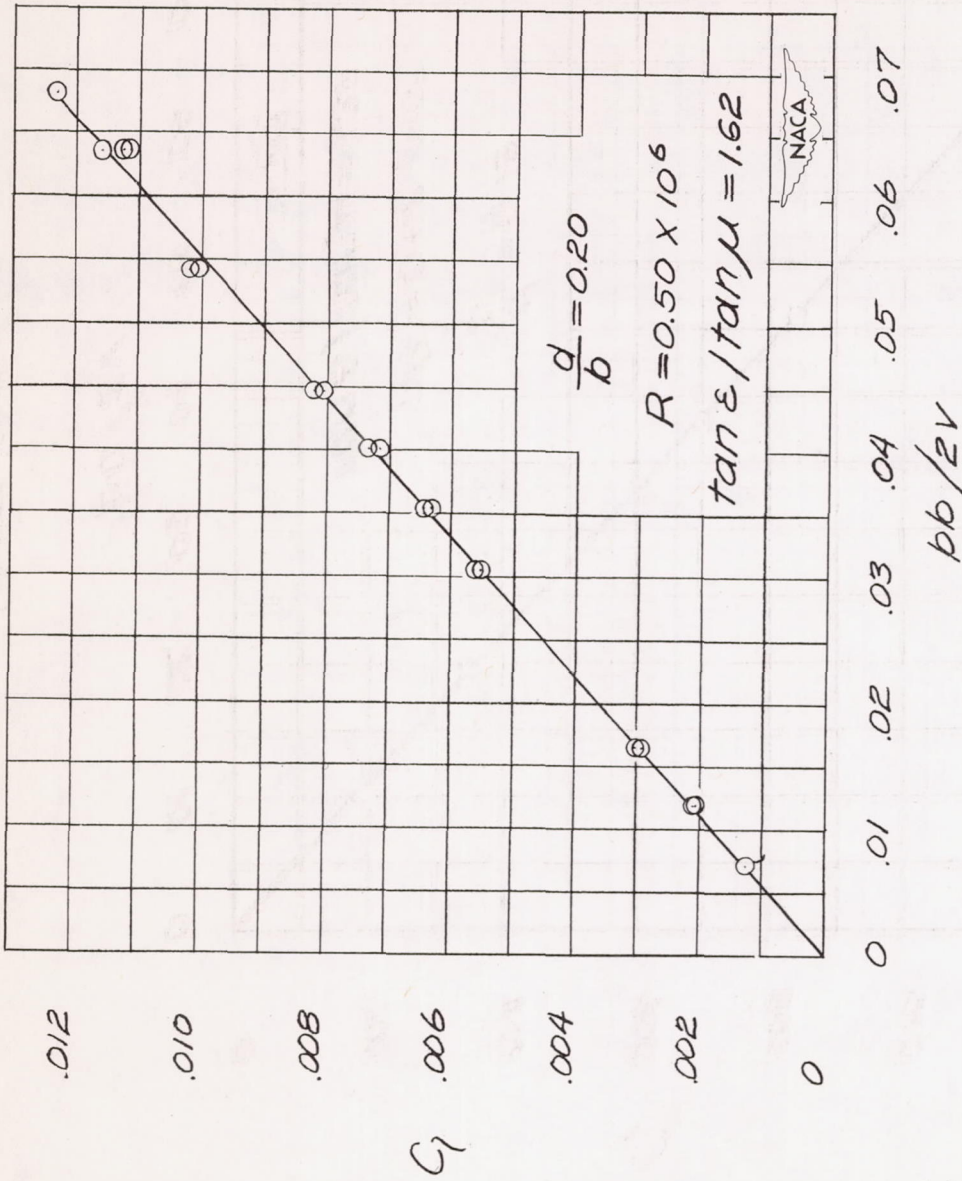
(h) Wing ε = 44.6°.

Figure 7.— Continued.

$$\frac{d}{b} = 0.20$$

$$R = 0.49 \times 10^6$$
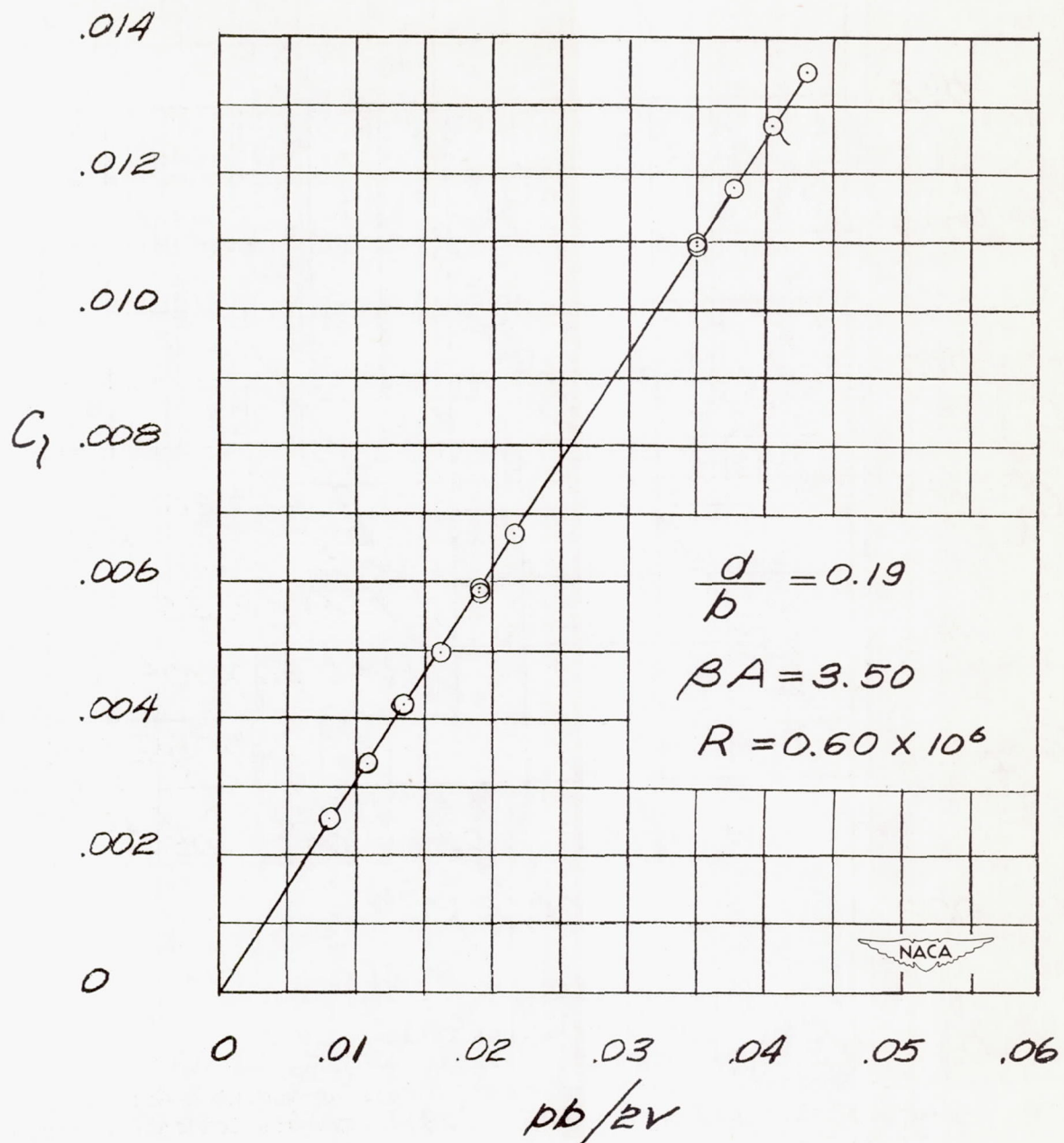
$$\tan \varepsilon / \tan \mu = 1.65$$
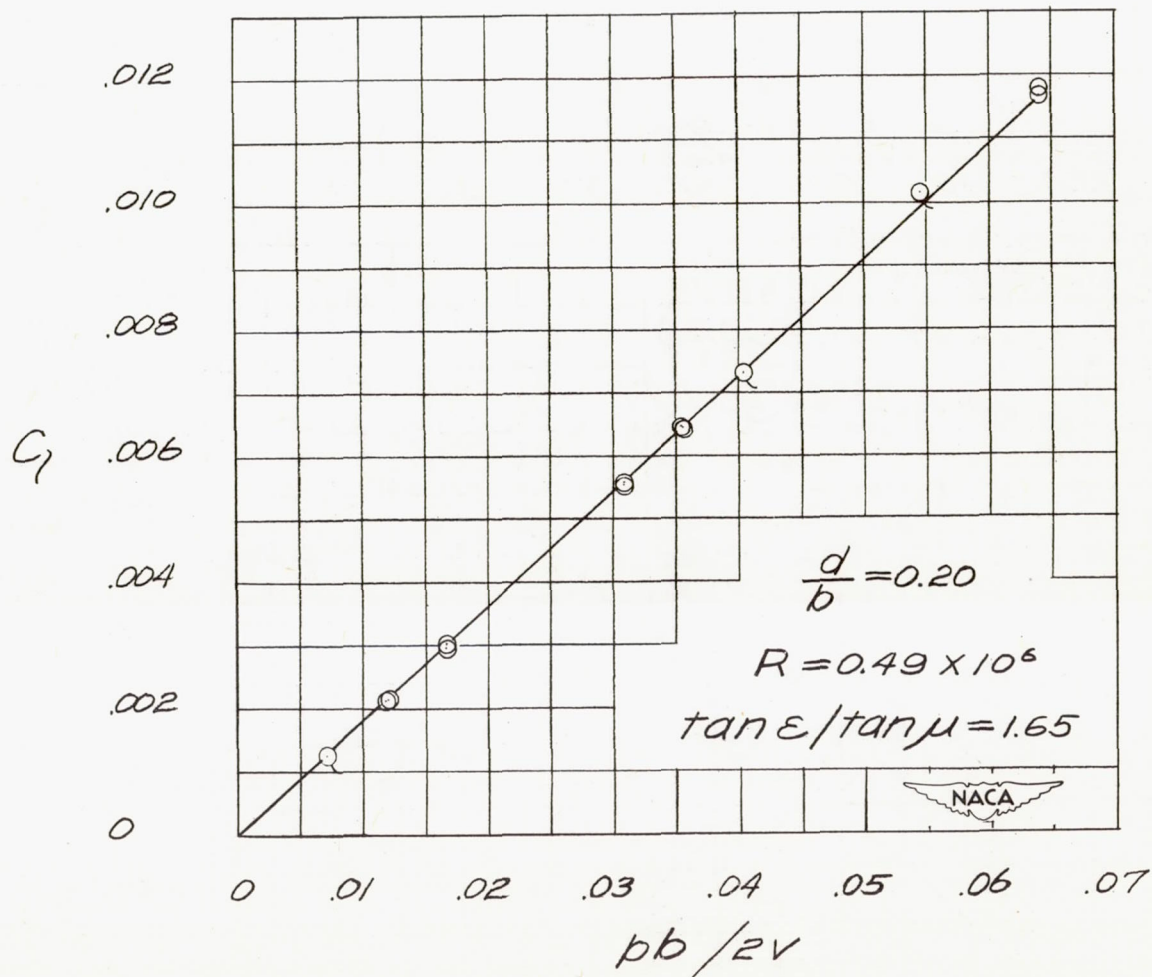
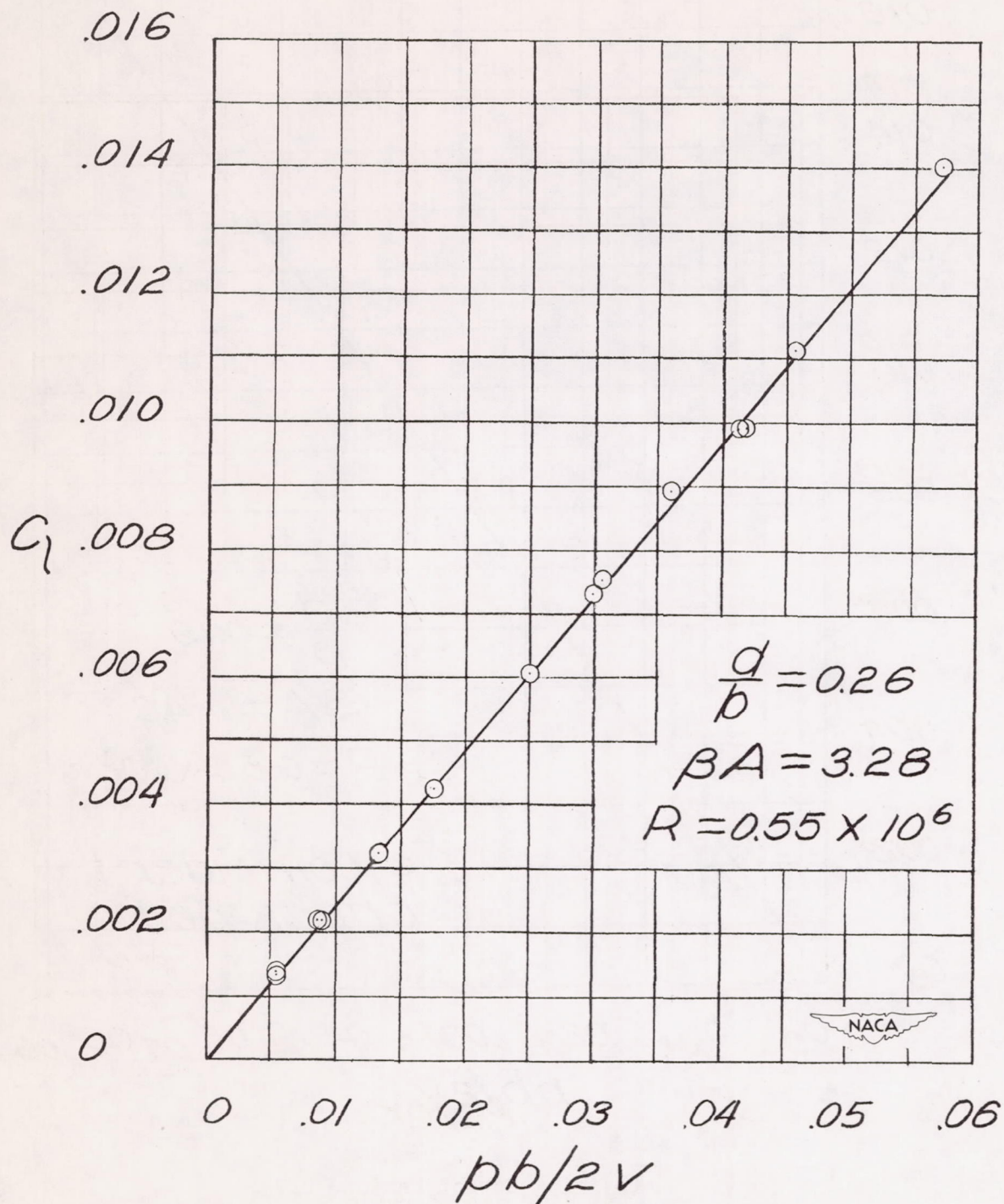(i) Wing $\varepsilon = 45.1^\circ$.

Figure 7.— Concluded.
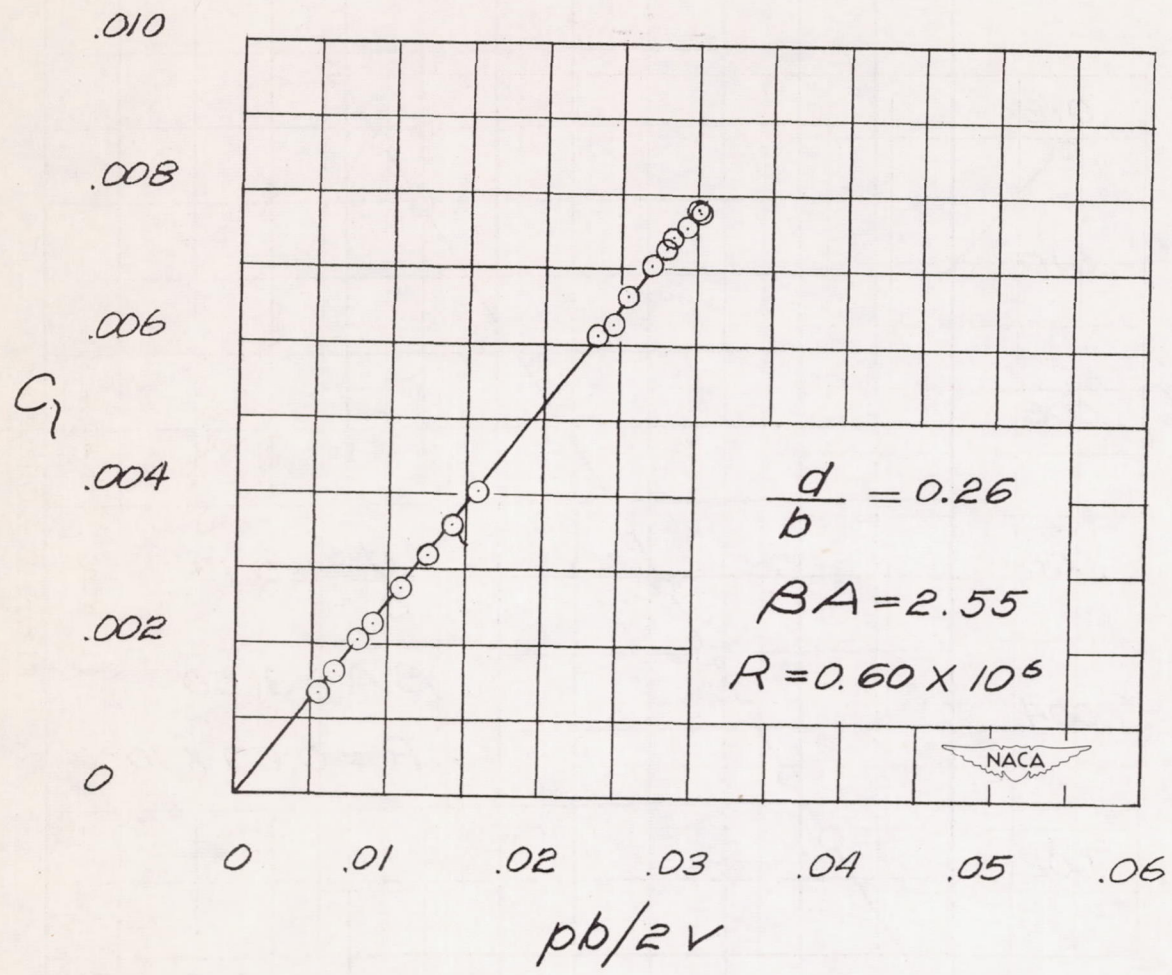
(a) Wing aspect ratio = 2.00.

Figure 8.— Rectangular-wing variation of rolling-moment coefficient with wing-tip helix angle. M = 1.62. (Tailed symbols indicate coincident check points.)
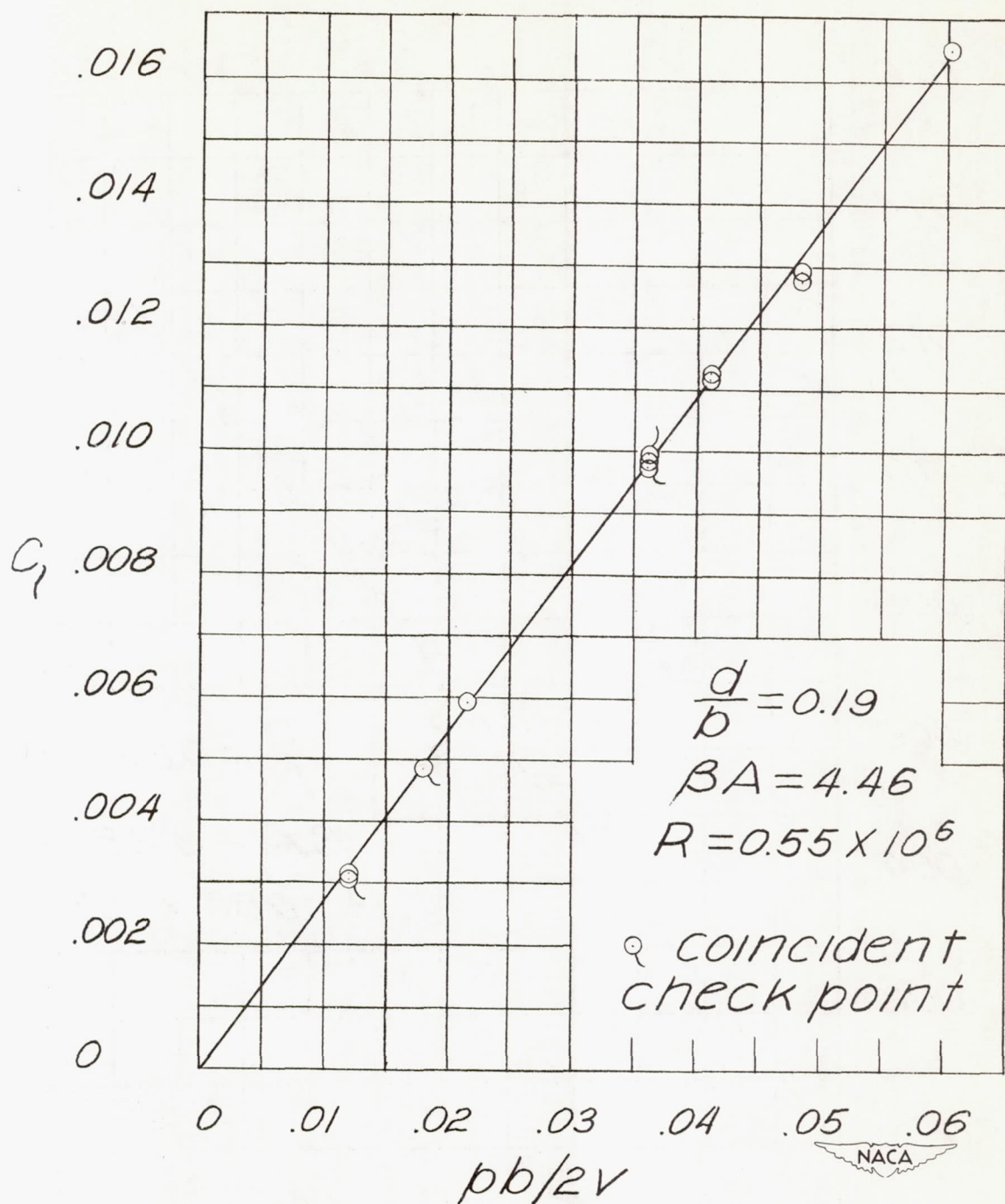
$$\frac{d}{b} = 0.19$$

$$\beta A = 3.50$$

$$R = 0.60 \times 10^6$$

(b) Wing aspect ratio = 2.73.

Figure 8.— Concluded.

$$\frac{d}{b} = 0.26$$

$$\beta A = 3.28$$

$$R = 0.55 \times 10^6$$

(a) Wing aspect ratio = 2.00.

Figure 9.— Rectangular-wing variation at rolling-moment coefficient with wing-tip helix angle.   M = 1.92.

(b) Wing aspect ratio = 2.73.

Figure 9.— Concluded.